EPFL

École Polytechnique Fédérale de Lausanne

Validation of the Serpent 2 model for the CARROUSEL facility

LABORATORY FOR REACTOR PHYSICS AND SYSTEMS BEHAVIOUR

Semester Project

Edoardo Luciano Brunetto

January 10, 2020

Contents

D Serpent2 script   **43**

Chapter 1

Introduction

The present report summarizes the work carried out between September and December 2019 at the Laboratory for Reactor Physics and Systems Behaviour at EPFL, in Lausanne. The work is targeted to the study of the neutronics of the CARROUSEL facility (Fig. 1.1), consisting of a Plutonium-Beryllium (PuBe) neutron source within an aluminium tank filled with water. It is used mainly for educational purposes and it is suitable for detectors characterization.
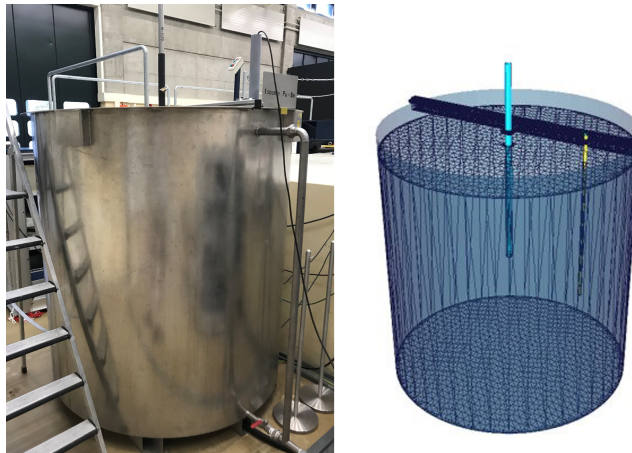
Figure 1.1: Picture and MCNP 3D model of the CARROUSEL facility [10]

The current work is based upon experimental measurements in the CARROUSEL facility and their comparison against Monte Carlo simulations performed via the transport code "Serpent 2" [6].

The main goals of the present study are:

- To convert the existing MCNP model for CARROUSEL in Serpent 2;

- To validate the Serpent 2 model with comparison against experimental data;

- To investigate the diffusion length in CARROUSEL as a "quick" parameter to test different detectors.

In addition, the ultimate intention of this work is to collect all the achieved results in a database, in order to provide a detailed description of the behaviour of the tested detectors in favour of further applications.

The present report is structured as follows:

- In Chapter 2 a detailed explanation of how the simulations are performed is given;

- Chapter 3 outlines the procedure with which measurements are conducted;

- In Chapter 4 the main outcomes of the present work are shown together with the validation procedure of the Monte Carlo model with experiments. The final part is dedicated to a focus on the diffusion length in CAR-ROUSEL, measured experimentally and simulated with Serpent 2.;

- In Chapter 5 conclusions on the main achievements of this work are drawn;

- In the Appendices data from experiments and simulations are transcribed, together with an example of the Serpent input code used for the simulations. Furthermore, mention is made to a preliminary study of the CARROUSEL energy spectrum.

Chapter 2

Serpent 2 model of the CARROUSEL facility

The Monte Carlo method obtains results by simulating individual particles and recordings some aspects of their average behaviour, without the need of solving any explicit equation. It considers all the possible reactions taking place as the particles travels in the medium using probability distributions. The process consists of following each of many particles from a source until its death in some terminal category (fission, absorption, escape etc.) [3].

In fact, no transport equations have to be formulated to determine the flux in a reactor. A number n of independent observations (neutron histories) are collected and the result is derived from the averaged observation. The method is widely used because of its efficiency in complex problems, without the need of simplifications. On the other hand, the main drawback is that the results will always be subjected to statistical errors. Indeed, as this error generally scales as $n^{-1/2}$, the computational cost can be a limiting factor [2].

In the work at hand the code used for the simulations was Serpent 2.1.29 [6], a three-dimensional transport code broadly employed in reactor physics applications. The cross section library used to perform all the simulation is JEFF 3.1.1. An example of the script used as input to run the simulations is given in Appendix D.

2.1 Geometry and materials

In order to run a Monte Carlo simulation, it is necessary to model the geometry of interest. In the case at hand, being CARROUSEL a simple tank of water, the modeled geometry represents the real one with a good level of approximation. As depicted in Fig.2.1 and 2.2, both the source and the tank have been modeled accurately, neglecting only the metallic support holding the instrumentation above the level of water, since it is deemed not relevant for the neutron economy. All the geometrical parameters have been taken from a preexisting work [10], since it is not trivial to measure some of them, especially when it comes to inner geometric details (e.g. the internal geometry of the PuBe source). An external volume of air surrounding the tank, which could be of interest for eventual analysis of radiation protection, is included in the geometrical model.
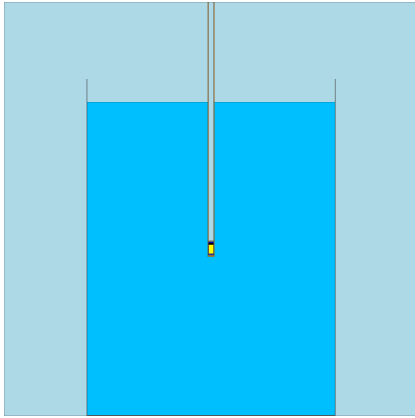
Figure 2.1: Geometric model of CAR-ROUSEL
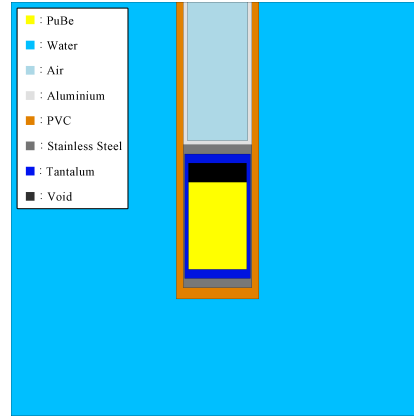
Figure 2.2: PuBe source geometry

The same preexisting work used for the geometry has been utilized for the materials definition [10].

2.2 Source characterisation

In the interest of having a suitable model, a proper energetic characterization of the neutrons source is essential. This represented a critical point in the modelling process, given the lack of information about the PuBe source of CARROUSEL. Moreover, it was not possible to determine experimentally its emission spectrum, and an alternative solution has been adopted. Two different energy emission spectra typical of PuBe sources are used in the simulations, respectively from [11] and [7]. All the simulation are therefore performed twice in order to collect data and to compare them afterwards with the experimental data. By comparing the simulation results with the experimental data it is possible to understand which of the two spectra approximate better the real PuBe source. A visual representation of the two emission spectra used for the simulations is portrayed in Fig. 2.3 and 2.4.
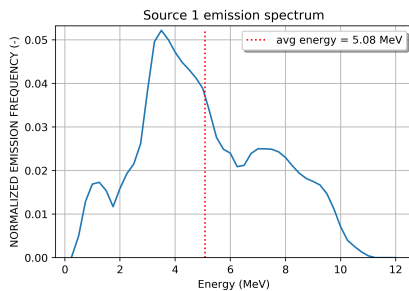
Figure 2.3: Emission spectrum according to [11]
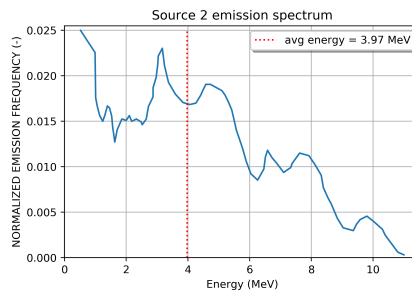
Figure 2.4: Emission spectrum according to [7]

4

2.3 Run parameters

Provided the stochastic nature of every Monte Carlo simulation code, parameters such as the choice of the number of neutrons to be simulated have to become an object of discussion. In this case, the criterion is to choose a suitable amount for which the consequent relative error on the reaction rates never exceed the order of few percents (5%). The selected value of neutrons to be simulated which was judged to be satisfactory is $1.5 \cdot 10^7$.

The strength of the source, i.e. the number of neutrons emitted per unit of time, was set equal to $5.03 \cdot 10^6 \frac{n}{s}$ as calculated in the aforementioned work [10].

2.4 Neutron detector models

With the purpose of scoring interactions of particles with the detectors, two different methods can be used in a simulation. The most accurate method consists in modeling the whole geometry of the detector (Fig. 2.5), and then run a simulation for each position at which the detector is moved. With this approach is possible to take into account the local flux perturbation caused by the detector, since the presence of a detecting species impacts locally on the neutron economy.

(a) ^3He_L

(b) $BF3$
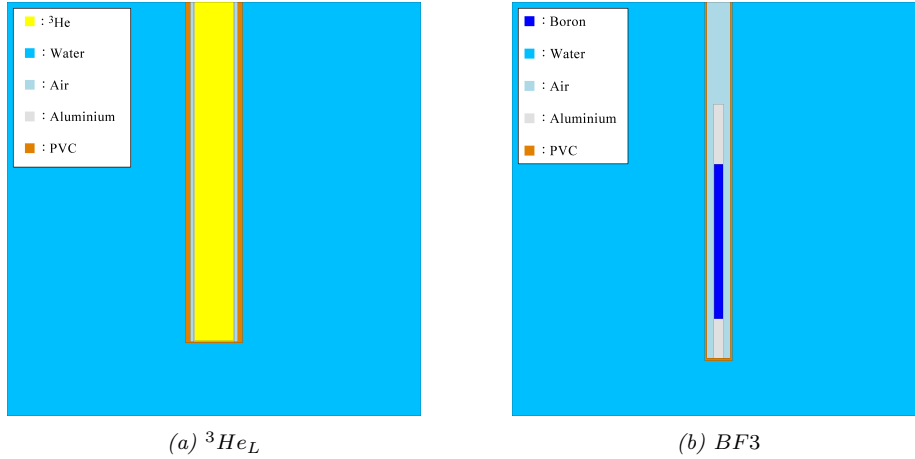
Figure 2.5: On the left, an ^{3}He detector and on the right, a BF_3 detector as modeled in Serpent 2.

Another procedure, equally significant but far more convenient, is to make use of the so called "virtual detectors". Employing this method, it is possible to define one or more volumes included in the preexisting geometry and use them to count the rate of interactions of neutrons with the detecting species. The reaction rate is computed as if the selected volume was filled with the detecting species, using for the computation a flux in absence of the detecting material. This reaction rate is computed from Serpent averaging on a specified volume as follow [5]:

$$R = \frac{1}{V} \int_V d^3r \int_{E_i+1}^{E_i} dE f(\mathbf{r}, E) \Phi(\mathbf{r}, E).$$ (2.1)

Both the response function $f(\mathbf{r}, E)$ and the spatial and energy domains of the integration are set by the detector parameters. In this work, several concentric cylindrical coronas are selected as a geometry for virtual detectors. The height and the thickness of the coronas were varied from case to case in order to better approximate the geometrical dimensions of each detector[1]. The volume in Eq.2.1 is set to unity by default, in order to have a total reaction rate (s^{-1}), and not the reaction rate density $(s^{-1}cm^{-3})$ as output.

Regarding the response function $f(\mathbf{r}, E)$, it is set in Serpent as an "ENDF reaction MT" which identifies a specific neutron reaction. In the simplest case, $f = 1$, the computation is reduced at the neutron flux integrated over space and energy. Instead, if a reaction cross section is included, the result is the corresponding reaction rate. In the case at hand, different reactions MTs (e.g. (n,p), (n,α)) are used depending on the detector used.

2.5 Performed simulations

To summarize, different types of simulations are performed for the present work. A first set of simulations, which had the objective to produce computational results to be compared with the experimental data, was run with virtual detectors. For all the detectors every simulation is run twice, implementing both of the two available source emission spectra. With these simulations it was possible to obtain computed count rates at any distance from the radioactive source for every detector. The count rates obtained were used both for the model validation and for the computed diffusion length evaluation.

Others simulations were performed at a preliminary stage of this work, to better characterize and understand the neutronics of CARROUSEL. To give an example, an evaluation of the energy spectra at different position was made (see Appendix A).

---

[1]Not valid for the ${}^3\text{He}_{\text{small}}$ for which the same model of the ${}^3\text{He}_{\text{large}}$ was used, being its inner dimensions unknown.

Chapter 3

Neutron detection measurements in CARROUSEL

Different detectors were used to record the neutron count rates at numerous distances from the radioactive PuBe source in CARROUSEL. Several measurements were carried out to be compared with the simulated results trying to maintain the measurements conditions as constant as possible. This objective has been pursued using the same read out electronics for each measurement (exception made for the fiber+scintillator detector).

The detectors used for collecting data are two gaseous proportional counters and an inorganic scintillator coupled with an optical fiber. The gaseous detectors consist of an ^{3}He detector, named in this work ^{3}He$_{small}$ and a BF_3 detector. Instead, the inorganic scintillator consists of a small scintillator screen made of ZnS:^{6}LiF with a sensitive area of 1 mm^2 coupled with an optical fiber for the signal transmission [12].

(a) BF_3
(b) ^{3}He$_{small}$
(c) Fiber + Scintillator (with the positioning tool inserted)
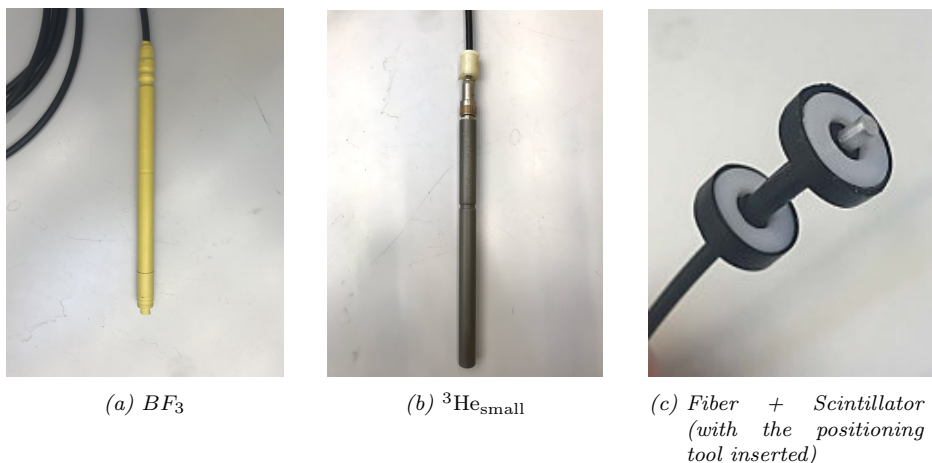
Figure 3.1: Pictures of the three detectors used.

3.1 Gaseous ionization chambers

The present section refers to the description of the experimental setup used for the measurements with the gaseous detectors, which represents the main part of the work at hand.
The read out electronics used for the gaseous detectors measurements is schematized in Fig.3.2.
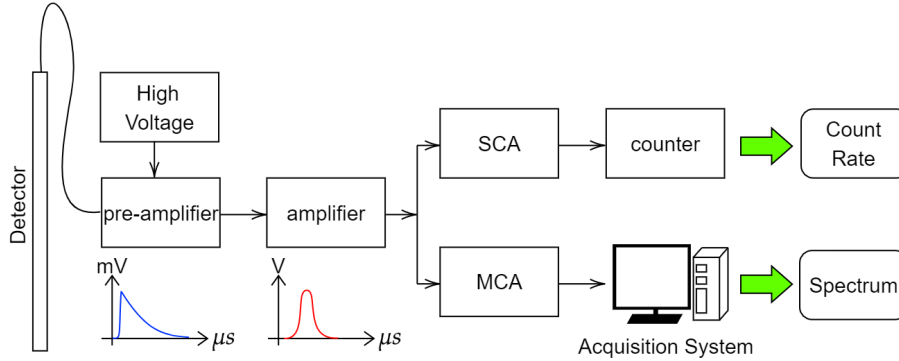
Figure 3.2: Simplified scheme of the read-out electronics in CARROUSEL

In addition to the components depicted in Fig.3.2, also a two-channel oscilloscope was used for the purpose of the signal visualization before and after the amplification process (see Fig.3.3).

In the gaseous detectors, the detection chain starts with a signal in current given by the detector when a particle (a neutron or a gamma in the present case) interacts with its detection species.
In the case of the gases used in the ionization chambers, the following reactions take place when a neutron interact with them:

$$^{10}_{5}\text{B} + ^{1}_{0}\text{n} \rightarrow \begin{cases} ^{7}_{3}\text{Li} + ^{4}_{2}\text{He} + 2.792\,MeV & (6\%) \\ ^{7}_{3}\text{Li}^{*} + ^{4}_{2}\text{He} + 2.310\,MeV & (94\%) \end{cases} \tag{3.1}$$

$$^{3}_{2}\text{He} + ^{1}_{0}\text{n} \rightarrow ^{3}_{1}\text{H} + ^{1}_{1}\text{H} + 764\,keV \tag{3.2}$$
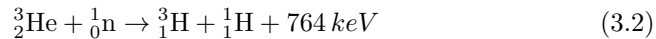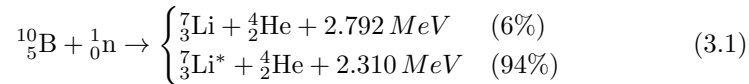
In this instance, the interaction consists of a neutral particle ionizing a gas and causing movement of charges towards the electrodes of the detector, to whom is applied a high tension voltage. The value of the HT voltage applied to the detectors varies from case to case, but in the present work it was always in the order of magnitude of 1 kV. The component responsible to supply the high voltage is the high voltage supply. The HV is provided to the detector through the pre-amplifier, which has also the task of transforming the current signal arriving from the detector to an impulse in tension through an RC circuit. The features of the pre-amplified signal are typically not acceptable, being its amplitude of few mV and considering the long decay tail (hundreds of μs) of the signal which is governed by the RC circuit time constant. These two characteristics are commonly undesirable in what concerns read-out signals since the amplitude of the signal is too weak to be properly read and the decay tail does not contain any useful information. Long decay tails can cause what is

Figure 3.3: Signals visualization in the oscilloscope (up: preamplified signal, down: amplified signal)
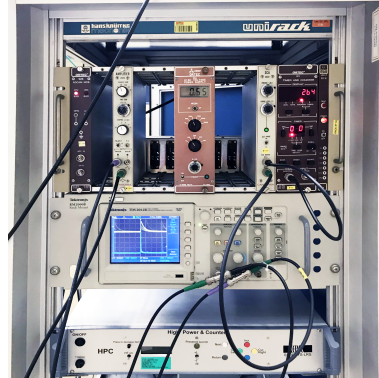
Figure 3.4: Photo of the utilized electronics

called "pile-up" phenomenon, i.e when two or more pulses happen in a time span that is shorter than the time needed to completely get rid of the decay tail of a previous signal. If the decay tail sums up with another pulse, the resulting amplitude is higher and not representative of the detected signal. Specifically when spectroscopy is the aim of the work, pile-up is absolutely to avoid.

In the current work, as shown in Fig.3.3, the preamplified signal was already enough short to avoid pile-up phenomena, thus there was no need to "cut" the decay tail through the amplifier. Nevertheless, the signal is processed in the amplifier in order to increase its amplitude up to few Volts. The signal is translated in a Gaussian-shape, as can be observed in Fig. 3.3. In order to have an appropriate amplification of the signals, several parameters of the amplifier need to be set. These are the gain, which is the ability of the amplifier to increase the voltage from the input port to the output port and the shaping time. The latter is representative of the time needed by the pulse to return to the baseline and has to be short enough to avoid pile-up phenomena. On the other hand, it must be kept longer with respect to the charge collection time of the detector, to avoid the loss of part of the amplitude. At the output of the amplifier the signal pass through the Single Channel Analyzer (SCA), which discriminate the signal. The discriminator produces an output logic pulse only if its input signal exceeds a preset threshold level. To give an example, if the threshold is set equal to 1 V, every signal falling below this limit are not interpreted by the discriminator as actual counts and are ignored. This is very useful to cut-off the signals induced by noise.

A procedure of threshold level determination is carried out for every measurement. It consists in counting the signal for a fixed amount of time with the threshold set to 0 V. Then the threshold is increased, and the number of counts for the same time span are expected to decrease. The process continues until the number of counts gets constant. Thereby all the noise is discriminated from the useful signals.

After the discrimination procedure, signals are transferred to a counter by way of which is possible to compute the count rate.

The detector spectrum is obtained through a Multi Channel Analyzer (MCA),

which distribute the signals in different channels according to their amplitude. The spectrum for each detector is visualized in a PC monitor through the software MAESTRO [9].

3.2   Miniature fiber-coupled scintillator

Count rates measurements in CARROUSEL are carried out also with an innovative detection system for highly localized measurements. The detector is made of three fundamental components: a scintillator+converter screen, an optical fiber and a Silicon Photon Multiplier (SiPM). The neutron interaction happens with the ^{6}LiF molecules (converter), which are responsible to convert thermal neutrons in charged particles according to the following reaction:

$$^6_3\text{Li} + ^1_0\text{n} \rightarrow ^3_1\text{H} + ^4_2\text{He} \tag{3.3}$$
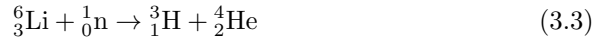
Light is generated from the interaction of charged particles with the ZnS molecules (scintillator) present in the screen together with ^{6}LiF in ratio 2:1. Part of this light is then collected and transported by an optical fiber to the SiPM, which generates an electrical signal by converting photons into electrons and by amplifying the signal.
Measurements with scintillator were carried out with a different read-out electronic system, which is widely described in [12] and depicted in the scheme of Fig.3.5.
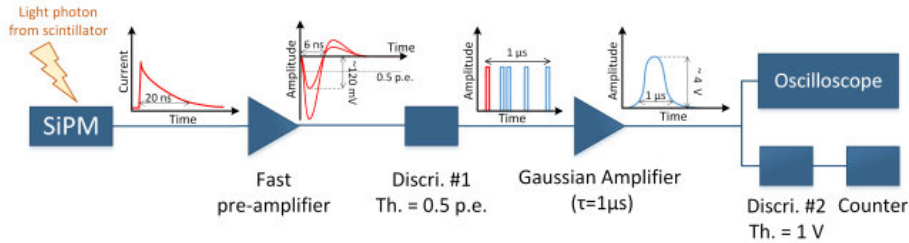
Figure 3.5: Read-out electronics used for the fiber+scintillator detector. [12]

It consists in a fast-preamplifier, which integrates the SiPM output signal (few tens of ns long) generating a negative output in the range of ns with an amplitude of hundreds of mV. Then, a fast-discriminator produces a square signal with a fixed amplitude when a signal corresponding to the detection of one or more photons reaches its input. The result is a train of pulses which increase in density when a neutron interacts with the scintillator. The train of pulses is processed by a Gaussian amplifier, which generates an output signal of 1 μs width with an amplitude in the range of few Volts, dependent upon the density of the train of pulses. The signal was then visualised through an oscilloscope and sent to a second discriminator stage, able to filter the square signals above a certain threshold amplitude which are then counted by a simple counter.

3.3   Performed measurements

To summarize, all the measurements performed for the work at hand have the objective to characterize the neutron count rates in CARROUSEL for several distances from the radioactive source. Measurements are carried out with the different kind of detectors described in the previous sections, with the hope of having a coherent description of the same phenomenon from measurement systems that relies on different physical principles.

Chapter 4

Results

4.1 Simulation results

All the results obtained through the Serpent 2 simulations are collected in an Excel spreadsheet and summarised in Appendix C. The document is divided in several pages, one for each detector, containing the computed reaction rates obtained at numerous distances from the source. The file contains the data obtained modeling both the source emission spectra available ([11] and [7]).

The aim of this document is to make available simulations data to be compared with experimental measurements in future works.
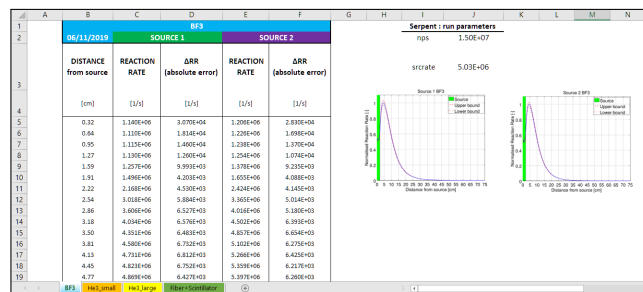
Figure 4.1: Screenshot of the Excel file where the simulated data are gathered.

All the notable results obtained from the simulations are shown in the following sections.

4.2 Experimental results

All the measurements data are gathered in an Excel file subdivided in sections, one for each detector tested. In the document the distances from the source, the number of counts registered, the time needed to reach the number of counts and the dead time of the detector (wherever was possible to see) are recorded. Others derived physical quantities are then reported in the same page, such as the count rate, the absolute error related to the number of counts and the

absolute error related to the count rate.

A summary of the collected data is available in Appendix B.
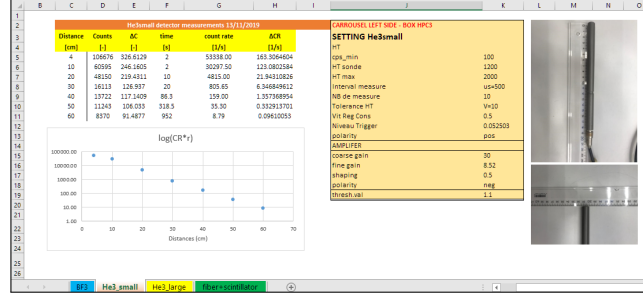
Figure 4.2: Screenshot of the Excel file where the measured data are gathered.

To compute the error on the number of counts it is used a property of the Poisson distribution.

As a matter of fact, when the number of nuclei in the sample is large and the observation time is short compared to the half-life of the radioactive species, Poisson distribution $P(n)$ represent properly the probability of observing a number of counts equal to n [4]:

$$P(n) = \frac{[E(n)]^n}{n!} e^{-E(n)} \tag{4.1}$$

where $E(n)$ is the expected value of counts.

Exploiting the Poissonic distribution property according to which the variance is equal to the expected value, it is possible to compute the standard deviation of the distribution as the square root of the expected value (i.e. the obtained number of counts). The computation of the absolute error is therefore performed as in Eq.4.2:

$$\sigma_{counts} = \sqrt{N_{counts}}. \tag{4.2}$$

For this reason it is possible to compute the number of counts needed to achieve a certain accuracy. In the case at hand, it was established as satisfactory a relative error of 1%, thus it follows from Eq.4.2 that at least 10^4 counts are needed.

4.2.1 Detector spectrum

Exporting the data collected through MAESTRO [9], it is possible to obtain the detector spectra at a given distance from the source. An energy calibration of the horizontal axis has been performed to obtain the energy information about all the channels of the spectrum. The two spectra portrayed in Fig.4.3 show by way of example the energy deposition peaks for the BF_3 and the $^3He_{small}$.
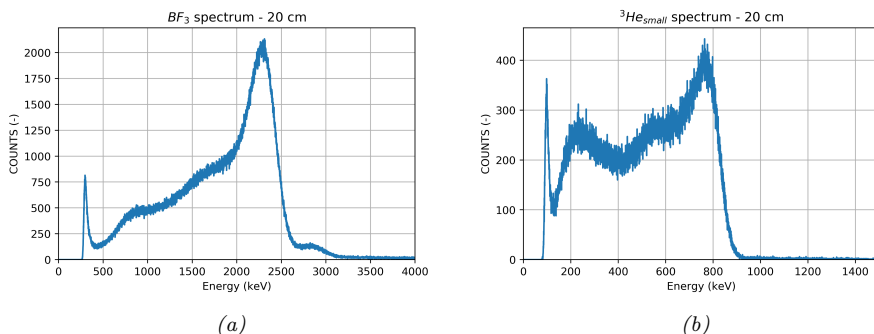
Figure 4.3: Spectra of BF3 (a) and $^3He_{small}$ (b) detectors

Some important information about reactions taking place in the detector can be deduced by looking at the spectra.

In the case of BF_3, the interaction of a neutron with Boron-10 (Eq. 3.1) can give rise to two different reactions, at which two different energies are associated. This is the reason why it is possible to observe two distinct peaks at 2.792 and 2.310 MeV. The amplitude of this peaks is proportional to the probability of the corresponding reaction to occur.

In the case of the ^{3}He, the interaction with a neutron consists in one possible reaction (Eq.3.2), that is the reason why only one peak is visible in the spectrum. The two plateaux visible in both the spectra are due to the "wall effect". When it comes to detector of finite dimension, it happens that a significant number of events involve energy loss in the detector wall rather than in the gas. From the conservation of energy and momentum it is possible to retrieve the energies of the charged particles generated. These energy represent the threshold limits of the wall-effect continuum corresponding to the situation where the neutron reaction occurs at the wall and only one of the particles can deposit its energy in the gas [3]. The peaks visible in both the spectra at low energies are due to electronic noise, and therefore they are cut-off with the procedure explained in Section 3.1.

4.2.2 Detector efficiency

With the measured count rates, it is possible to compute the efficiency for every detector. In order to obtain an index of performance which is not reliant on a specific neutron source or on a specific geometry, the optimal choice would be computing the intrinsic efficiency for each detector (Eq.4.3).

$$\epsilon_{int} = \frac{Detector\,reading}{Number\,of\,radiation\,quanta\,incident\,on\,detector} \tag{4.3}$$

A Monte Carlo simulation can determine what the reaction rate of a given detector is at a specific distance from the source (i.e. the denominator of Eq.4.3). Nevertheless, what makes this computation impossible in this work is the absence of reliable data on the densities of the gaseous species in the proportional counters. Because of the absence of these data it is not possible to calculate the reaction rates as shown in Eq.4.4.

$$RR = N_{gas} \cdot \sigma_{reaction} \cdot \Phi \tag{4.4}$$

14

4.3 Validation of the model

With the purpose of assessing the goodness of the model, a validation procedure is necessary. To validate the Monte Carlo model, Serpent 2 [6] is used to compute the count rates for every detector at several distances from the source and then data are compared with experimental points measured in CARROUSEL.

As portrayed in Fig.4.4, the model characterize with accuracy the behaviour of the detectors in CARROUSEL. The simulation data are obtained for both the available source spectra, labelled in the plots as "Source1" and "Source2".

Both the errors on measurements and simulations are represented in the plots, even if not clearly visible given their small value (see Appendix B and C for the values).

(a)

(b)

(c)
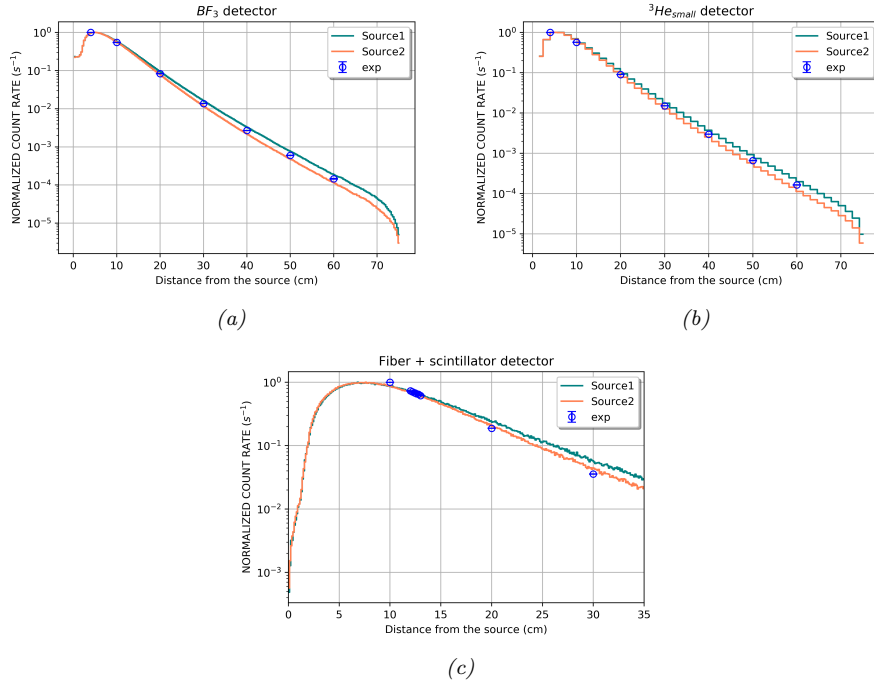
Figure 4.4: Comparison between experimental and simulated results.

In Fig.4.4 is shown the normalized count rates as a function of the distance from the source. The logarithmic scale used for the y-axis allows to show the linearity of the curves, which comes from the solution of the diffusion equation in radial coordinates for a point source in a non-multiplying medium (see Section 4.4.1). In order to have an objective criterion to determine the goodness of the simulations approximation for the experiments, the "$\frac{C}{E} - 1$" parameter is computed. Since C stands for the computed results ad E for the experimental data, this parameter is supposed to be equal to zero when experiments and simulation are perfectly in agreement.

The parameter is computed for different detectors and for all the available experimental points (see Fig.4.5).
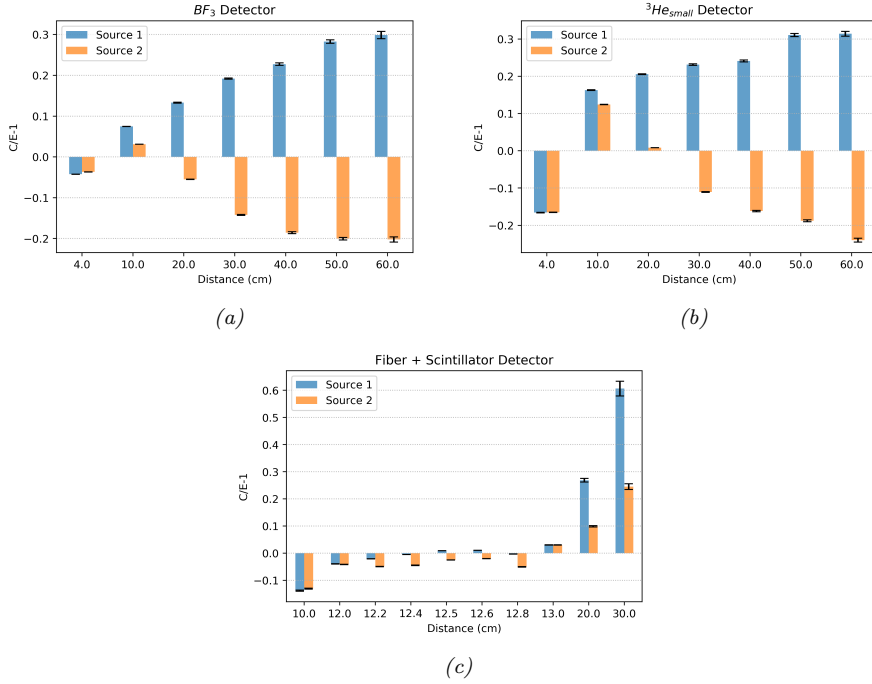
Figure 4.5: C/E-1 parameter for different detectors

As shown in Appendix C, by using virtual detectors the simulations give as output the reaction rates computed for every defined bin. Knowing that every bin has a radial extension, the output value is averaged on the whole bin, from the inner to the outer radius. The same averaging concept is intrinsic in the measurements procedure when it comes to real detector. Anyway, in the present work the value taken as "Distance" is the central value of every bin, considered to be representative of the average reaction rate of the bin.

As depicted in Fig.4.5, all of the three detectors show a similar trend. The discrepancy between experiments and simulations seems to increase more than 20% after 30 cm. The data obtained through the fiber prove to be particular in agreement with the simulations, with a relative difference of $\pm$ 5% for the distances between 12 and 13 cm away from the source.

4.4 Validation of the diffusion length

As mentioned in Chapter 1, one of the objectives of the present work is to assess the diffusion length in CARROUSEL.
The diffusion length is obtained from the solution of the Neutron Diffusion Theory, which describes under some hypotheses and simplifications the behaviour of neutrons in a medium. From a physical point of view, the diffusion length corresponds to the distance travelled by a neutron from the moment it becomes thermal to the moment it is absorbed. So the bigger the diffusion length is, the more diffusive and less absorptive the medium is.

An important remark which needs to be done regards the validity of the

16

Diffusion Theory. In fact, the derivation of diffusion equation depends on Fick's law, which provides the relationship between neutron flux Φ and neutron current J. Given that Fick's law is obtained under several assumptions, the Diffusion theory has limits of applicability. Indeed, its solution can be obtained for simple systems under the simplifications of monoenergetic, isotropic and point source. Unfortunately, not all the above mentioned hypotheses can be considered suitable for the case at hand. The main discrepancy is that the PuBe source of CARROUSEL cannot be approximated as monoenergetic. As a matter of fact, having neutrons born at high energies (see Fig. 2.3 and 2.4) means that they will need a certain distance to collide and become thermals. This implies that from the energetic point of view there will be a thermal neutron source distributed over all the water domain, since neutrons are born from the slowing down of fast neutrons everywhere in CARROUSEL.

Hence, to be fair, what we are referring to as "diffusion length" has not exactly the meaning it is supposed to have. For the aforementioned reasons, in the present work a higher value with respect to the reference one for water (2.725 ± 0.03 cm [1]) is expected. This does not mean that the distance travelled by a thermal neutron to be absorbed is different from 2-3 cm in CARROUSEL, but it is because the parameter computed here is more related to the average distance covered by neutrons from their birth to their absorption. The higher the energy of a neutron, the longer the distance needed to be absorbed in water.

In the present work, diffusion length is evaluated both through experiments and simulations in order to compare data.

4.4.1 Experimental diffusion length

The starting point for the diffusion length computation is the diffusion equation, here in radial coordinates because of CARROUSEL geometry:

$$D\nabla^2\Phi(r) - \Sigma_a\Phi(r) = S \tag{4.5}$$

where D is the diffusion coefficient, Σ_a is the macroscopic absorption cross section and S is the source. Under the assumptions of point and isotropic source with monoenergetic neutron emission the well known solution for the flux is obtained:

$$\Phi(r) = \frac{S}{4\pi Dr}e^{-r/L} \tag{4.6}$$

where L is the diffusion length. Then, considering proportionality between count rate and neutron flux, one can write the following relation:

$$ln(CR \cdot r) = -\frac{r}{L} + const \tag{4.7}$$

which represents a line on the plane $(r, ln(CR \cdot r))$ with a slope equal to $-\frac{1}{L}$. Then, the derivation of the value of L is straightforward.
The collected experimental points has been fitted with a suitable MATLAB [8] tool in order to get the analytical expression for the above mentioned function (Eq. 4.7).

This method yields to the results of Figure 4.6a and 4.6b, in which are represented by way of example the data collected for two detectors : BF_3 and ^3He small.
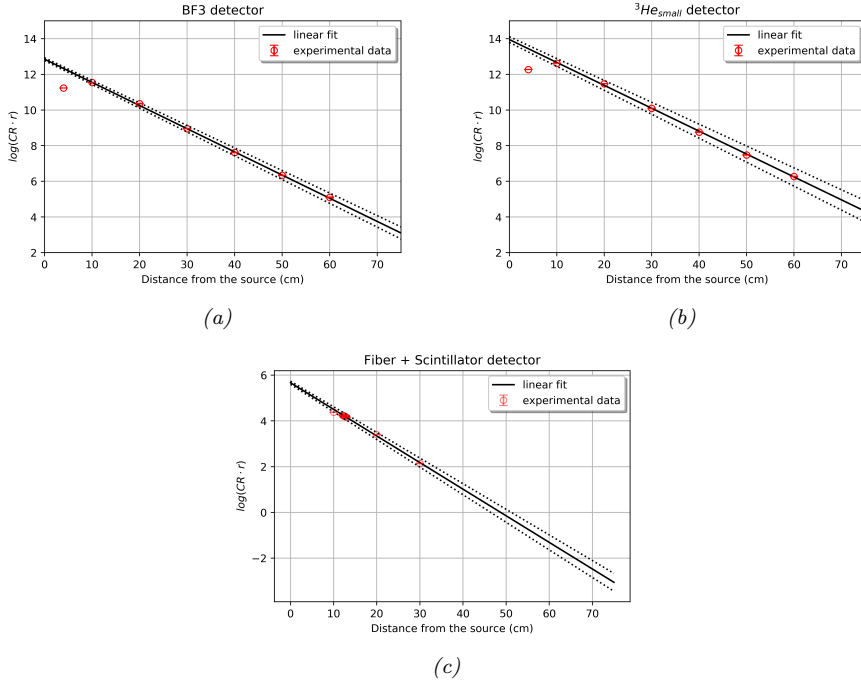
Figure 4.6: Measurements with BF_3 and $^3He_{small}$

As pointed out in the plots, the experimental data have a linear behaviour, as described by the solution of the diffusion equation. Only the measurements at the closest point to the source are misaligned, due to the prevalence of fast neutrons in this region (see Appendix A). This effect could also be explained as a loss of the "point source" hypothesis, since the measurement is performed too close to the source.

The numerical values resulting from these measurements are summarized in Table 4.1.

4.4.2 Simulated diffusion length

In order to compare the measured values, simulation in Serpent 2 [6] are carried out with each detector. The source emission spectrum used in the simulation is that named "Source 2" [7], since it approximates better the experimental data (see Fig.4.5). Just as in the experimental case, only the linear part of the curve is taken into account to fit the simulated data.

(a)

(b)

(c)
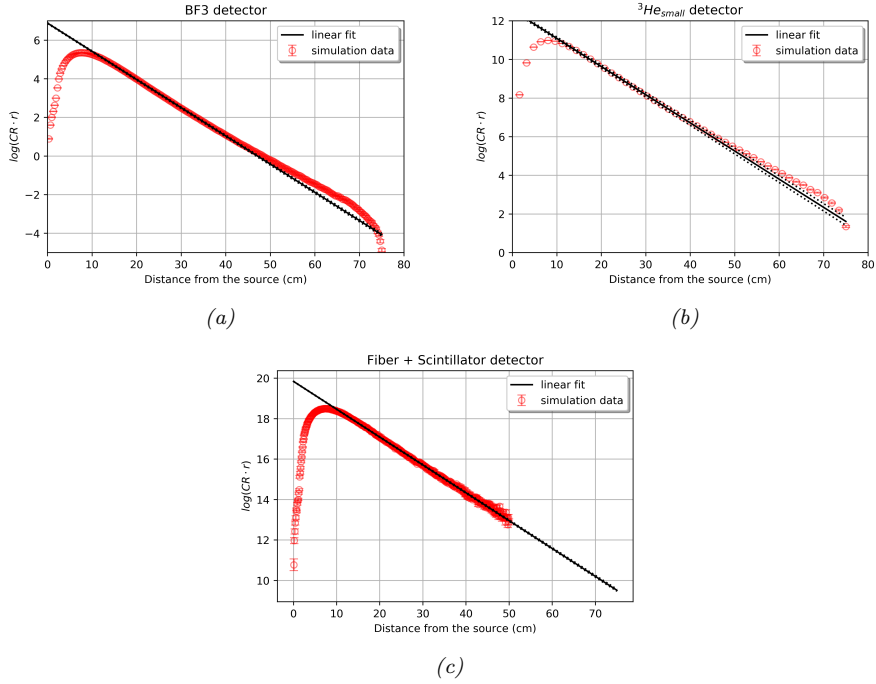
Figure 4.7: Diffusion length from simulations

In Fig.4.7 is depicted the linear fit performed to retrieve the diffusion length from BF_3, ${}^3He_{small}$ and fiber simulations. Despite the good linear trend of the curves, it is possible to notice a mild loss of linearity towards the boundary of CARROUSEL, in which the curve is above the fitting line. To verify if it can be considered an effect of the boundary, a simulation without boundaries is performed. A new test model called "unbounded CARROUSEL" is used for this assessment, created by removing the Stainless Steel boundaries and extending the water region up to a radius of 1 m. The results, obtained through BF3 virtual detectors, are shown in Fig.4.8. With the unbounded model the curvature effect previously present disappears. Therefore, the loss of linearity could be caused by the reflection of part of the neutrons from the Stainless Steel (SS) tank. Nevertheless, the SS is known to be a good reflector for fast or epithermal neutrons, and should be transparent to thermal ones. For this reason, further investigation on this aspect should be carried over.
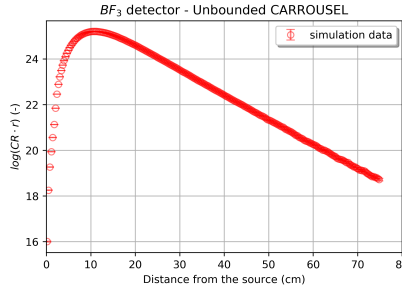
Figure 4.8: Assessment on the boundaries effect

Again, the simulated results for the diffusion length are listed in Tab. 4.1.

4.4.3 Comparison between simulations and experiments

Data regarding the measured and the simulated diffusion length are compared in Tab. 4.1.

Table 4.1: Diffusion lengths comparison

Detector	Measurements (cm)	Simulations (cm)	C/E-1 (%)
BF_3	7.7 ± 0.2	6.96 ± 0.04	10.6 ± 0.3
$^3He_{small}$	7.8 ± 0.4	7.02 ± 0.07	11.1 ± 0.6
$Fiber$	8.6 ± 0.3	7.26 ± 0.03	18.5 ± 0.6

As emphasized by Fig.4.9 all the measured diffusion lengths are in the same range of uncertainty, apart from the fiber which yields a result 10% higher than the other detectors.

As already done for the validation procedure, the parameter C/E-1 is computed to have a clear parameter to compare the data (see Tab.4.1).
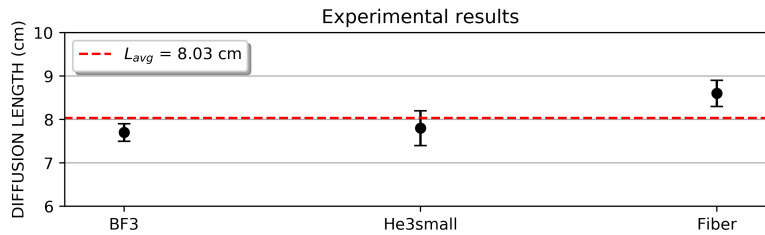
Figure 4.9: Experimental diffusion lengths

The higher value resulting from the fiber measurements could be explained by the different readout electronics utilized, which details are available in Appendix B. Moreover, in the case of the fiber count rates are measured at less distances, since the focus was shifted on the minimization of the error. In fact, fiber's measurements are performed with at least $2 \cdot 10^4$ counts, in order to guarantee an error smaller than 1 % after normalization procedures.
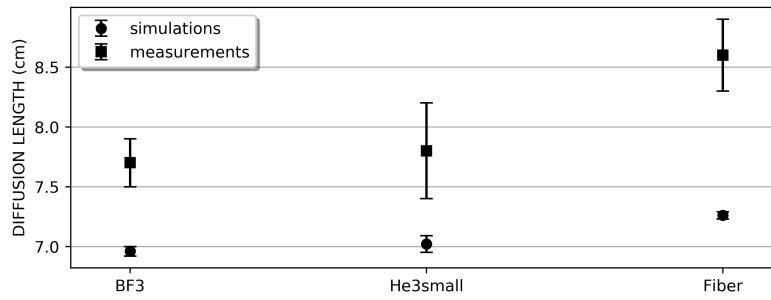
Figure 4.10: Comparison diffusion lengths

Figure 4.10 shows that the computed diffusion lengths are not included in the range of uncertainties of the measured data, and overall they under-predict the experimental results.

This might be caused by the spatial self-shielding effect introduced by the detector positioning. In fact, the presence of the detector induces a flux perturbation which is not taken into account in the simulations, where virtual detectors are used.

Chapter 5

Conclusions

The main objectives persecuted in this work, focused on the study of the CAR-ROUSEL neutronics, have been achieved. The available MCNP model for CAR-ROUSEL has been successfully converted in a Serpent2 model and validated through experimental data. The validation procedure has shown an acceptable level of agreement between the experiments and the simulations, with a maximum C/E-1 value of 30% (exception made for the farthest fiber measurement). The diffusion length investigation has led to a closer analysis of the neutrons behaviour in the facility, giving information on energetic features of the PuBe source, even if its exact emission spectrum is still not known. Also in the case of the diffusion length, the agreement between simulations and experiments was satisfactory, with a C/E-1 value always lower than 20%.

The main limitations, that precluded the possibility to define the intrinsic performance parameters for the detectors, were caused by the absence of reliable data on the state variables of the gases contained in the ionization chambers. Nevertheless, even if not all the objectives pursued in the current work have been met, progress has been made in the characterization of the studied detectors, by making available useful data for future studies.

Appendices

Appendix A

Energy spectrum in CARROUSEL

The content of this section is part of a preliminary assessment made on CARROUSEL to better understand how the energy spectrum of the neutron population varies with the distance from the source. Spectra are obtained through a Serpent simulation using virtual detectors with an energy grid from 10^{-11} to $2 \cdot 10^1$ MeV for the spectroscopy.

By analyzing the spectra, it is possible to understand at which distance from the source the neutron population is mainly dominated by the presence of thermal or fast neutrons.
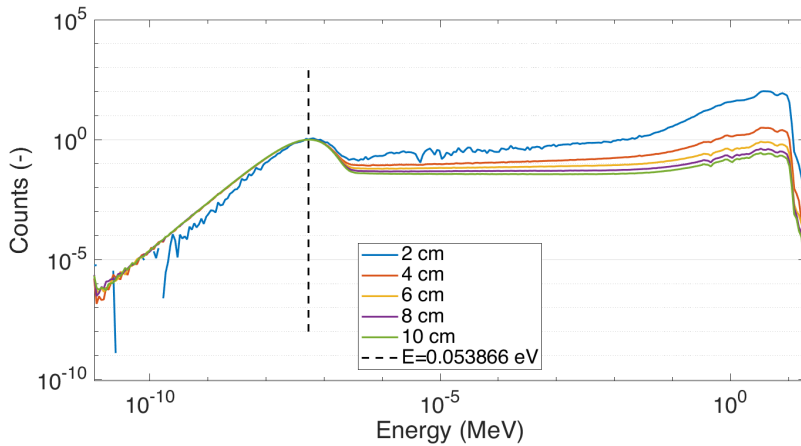
Figure A.1: Energy spectra at different distances from the source

Figure A.1 shows a predominant fraction of fast neutron at the source interface (2 cm), caused by the nature of the source spectrum implemented in this model ([11]) which emits neutrons with an average energy of 5 MeV (see fig.2.3). Although a thermal peak is already visible at 2 cm, it represents only 1% of the fast neutron population. On the contrary, the spectrum at 10 cm shows a thermal peak about one order of magnitude bigger than the fast one.

The fact that the thermal fraction of neutrons close to the source is small but non negligible, is probably due to back-scattering effect, which causes the reflection of some neutrons back to the region adjacent to the source. In fact, since the diffusion length in water is approximately 3 cm [1], it is unlikely that 1% of neutrons is already become thermal at the interface of the source surface and the water.

From fig.A.1 it is also appreciable the Maxwellian distribution of energies assumed by the neutrons in the thermal region.

Appendix B

Experimental data

All the experimental data collected in the CARROUSEL facility are reported hereafter. For the sake of clarity the following tables contain only the distances from the PuBe source, the counts and the time needed to carry over the measurement. All the other physical quantities used in the work at hand can be retrieved from these data. Together with the measured data, also the settings of the used readout electronics are briefed in an apposite table.

B.1 $^3\text{He}_{large}$ proportional counter

$^3\text{He}_{large}$ detector - 15.11.2019		
Distance from PuBe source (cm)	Counts (-)	Time (s)
6	10113	45.4
10	10160	12.4
12.5	10551	4.2
15	18193	1.6
20	19915	0.8
30	10867	2.7
40	10324	11.8
50	10154	50.4
60	10018	206.9

Table B.1: Experimental data for $^3\text{He}_{large}$ detector

Electronics setting parameters		
Coarse gain	300	-
Fine gain	5	-
Shaping time	8	μs
High tension	1060	V
Threshold MCA	0,8	V

Table B.2: Electronics settings for $^3\text{He}_{large}$ detector

B.2 BF_3 proportional counter

BF_3 **detector** 31.10.2019		
Distance from PuBe source (cm)	Counts (-)	Time (s)
4	188887	10
10	103192	10
20	15661	10
30	25801	100
40	10110	199,7
50	10178	900,7
60	2247	821,1

Table B.3: Experimental data for BF₃ detector

Electronics setting parameters		
Coarse gain	30	-
Fine gain	12.8	-
Shaping time	1	μs
High tension	1600	V
Threshold MCA	1	V

Table B.4: Electronics settings for BF₃ detector

B.3 $^3\mathrm{He}_{small}$ proportional counter

$^3\mathrm{He}_{small}$ **detector - 13.11.2019**		
Distance from PuBe source (cm)	Counts (-)	Time (s)
4	106676	2
10	60595	2
20	48150	10
30	16113	20
40	13722	86.3
50	11243	318.5
60	8370	952

Table B.5: Experimental data for $^3\mathrm{He}_{small}$ detector

Electronics setting parameters		
Coarse gain	30	-
Fine gain	8.5	-
Shaping time	0.5	μs
High tension	1200	V
Threshold MCA	1.1	V

Table B.6: Electronics settings for $^3\text{He}_{small}$ detector

B.4   Fiber + scintillator

Fiber + scintillator detector - 13.11.2019		
Distance from PuBe source (cm)	Counts (-)	Time (s)
10	433742	54470.3
12	20113	3440.8
12,2	21120	3736.7
12,4	20482	3754.5
12,5	36162	6754.6
12,6	20018	3819.3
12,8	20013	3889.8
13	20174	4119.4
20	24499	16355.4
30	18550	65454.6

Table B.7: Experimental data for fiber + scintillator

Electronics setting parameters		
Coarse gain	30	-
Fine gain	0.5	-
Shaping time	1	μs
SiPM Voltage	56.5	V
Preamp Voltage	6	V
Th. 1st discriminator	0.5	p.e.
Th. 2nd discriminator	1	V

Table B.8: Electronics settings for fiber + scintillator

Appendix C

Simulation data

In this chapter are provided the output data of the Serpent2 simulations for each detector. Both the outputs considering the two available source spectra ([11] and [7]) are here summarized.

A detailed description of how these data are obtained is given in Appendix D. All the reaction rates provided by Serpent2 are given in $\frac{b \cdot cm}{s}$, since a multiplication by the detector species density is required to obtain the RR in $\frac{1}{s}$ [5]. As they are, these data can be used for a comparison with experimental points after normalization procedures.

	BF_3			
	S1		S2	
Distance (cm)	RR_{sss2} $\frac{b \cdot cm}{s}$	err (-)	RR_{sss2} $\frac{b \cdot cm}{s}$	err (-)
0.16	5.38E+07	2.69%	5.68E+07	2.35%
0.48	1.57E+08	1.63%	1.73E+08	1.38%
0.79	2.63E+08	1.31%	2.92E+08	1.11%
1.11	3.73E+08	1.12%	4.14E+08	0.86%
1.43	5.33E+08	0.80%	5.85E+08	0.67%
1.75	7.76E+08	0.28%	8.58E+08	0.25%
2.07	1.33E+09	0.21%	1.49E+09	0.17%
2.38	2.13E+09	0.19%	2.38E+09	0.15%
2.70	2.89E+09	0.18%	3.22E+09	0.13%
3.02	3.61E+09	0.16%	4.03E+09	0.14%
3.34	4.31E+09	0.15%	4.81E+09	0.14%
3.65	4.97E+09	0.15%	5.53E+09	0.12%
3.97	5.58E+09	0.14%	6.21E+09	0.12%
4.29	6.14E+09	0.14%	6.82E+09	0.12%
4.61	6.66E+09	0.13%	7.38E+09	0.12%
4.93	7.13E+09	0.13%	7.88E+09	0.11%
5.24	7.53E+09	0.13%	8.32E+09	0.10%
5.56	7.87E+09	0.13%	8.68E+09	0.10%
5.88	8.16E+09	0.14%	9.00E+09	0.10%
6.20	8.41E+09	0.13%	9.24E+09	0.10%
6.51	8.60E+09	0.13%	9.43E+09	0.10%

6.83	8.74E+09	0.13%	9.56E+09	0.09%
7.15	8.84E+09	0.13%	9.65E+09	0.09%
7.47	8.90E+09	0.13%	9.69E+09	0.10%
7.79	8.93E+09	0.12%	9.68E+09	0.09%
8.10	8.92E+09	0.12%	9.64E+09	0.10%
8.42	8.87E+09	0.12%	9.56E+09	0.10%
8.74	8.79E+09	0.12%	9.45E+09	0.10%
9.06	8.68E+09	0.11%	9.30E+09	0.10%
9.38	8.56E+09	0.11%	9.15E+09	0.09%
9.69	8.43E+09	0.11%	8.97E+09	0.10%
10.01	8.27E+09	0.11%	8.77E+09	0.10%
10.33	8.09E+09	0.11%	8.55E+09	0.10%
10.65	7.90E+09	0.12%	8.32E+09	0.10%
10.96	7.70E+09	0.11%	8.09E+09	0.09%
11.28	7.49E+09	0.11%	7.86E+09	0.10%
11.60	7.28E+09	0.12%	7.60E+09	0.10%
11.92	7.08E+09	0.12%	7.35E+09	0.10%
12.24	6.86E+09	0.12%	7.09E+09	0.10%
12.55	6.64E+09	0.12%	6.84E+09	0.11%
12.87	6.42E+09	0.13%	6.58E+09	0.11%
13.19	6.22E+09	0.13%	6.33E+09	0.11%
13.51	6.01E+09	0.13%	6.09E+09	0.11%
13.82	5.79E+09	0.13%	5.84E+09	0.11%
14.14	5.58E+09	0.14%	5.61E+09	0.12%
14.46	5.38E+09	0.15%	5.39E+09	0.13%
14.78	5.17E+09	0.14%	5.17E+09	0.12%
15.10	4.98E+09	0.15%	4.95E+09	0.12%
15.41	4.80E+09	0.15%	4.74E+09	0.13%
15.73	4.61E+09	0.16%	4.53E+09	0.12%
16.05	4.43E+09	0.16%	4.34E+09	0.13%
16.37	4.26E+09	0.16%	4.14E+09	0.14%
16.68	4.09E+09	0.17%	3.96E+09	0.14%
17.00	3.92E+09	0.16%	3.79E+09	0.15%
17.32	3.77E+09	0.16%	3.61E+09	0.14%
17.64	3.61E+09	0.18%	3.45E+09	0.16%
17.96	3.47E+09	0.19%	3.29E+09	0.16%
18.27	3.32E+09	0.19%	3.14E+09	0.15%
18.59	3.19E+09	0.20%	3.00E+09	0.15%
18.91	3.05E+09	0.20%	2.85E+09	0.16%
19.23	2.93E+09	0.21%	2.73E+09	0.17%
19.54	2.80E+09	0.21%	2.60E+09	0.18%
19.86	2.69E+09	0.20%	2.48E+09	0.18%
20.18	2.57E+09	0.21%	2.36E+09	0.17%
20.50	2.47E+09	0.22%	2.25E+09	0.18%
20.82	2.36E+09	0.24%	2.14E+09	0.19%
21.13	2.26E+09	0.22%	2.04E+09	0.20%
21.45	2.16E+09	0.22%	1.94E+09	0.21%
21.77	2.07E+09	0.23%	1.85E+09	0.22%
22.09	1.98E+09	0.22%	1.76E+09	0.22%
22.40	1.90E+09	0.22%	1.68E+09	0.23%

22.72	1.82E+09	0.22%	1.60E+09	0.23%
23.04	1.75E+09	0.22%	1.53E+09	0.25%
23.36	1.67E+09	0.24%	1.46E+09	0.25%
23.68	1.60E+09	0.25%	1.39E+09	0.24%
23.99	1.53E+09	0.25%	1.33E+09	0.26%
24.31	1.47E+09	0.24%	1.27E+09	0.27%
24.63	1.41E+09	0.25%	1.21E+09	0.26%
24.95	1.35E+09	0.27%	1.15E+09	0.27%
25.26	1.29E+09	0.28%	1.10E+09	0.27%
25.58	1.24E+09	0.29%	1.05E+09	0.27%
25.90	1.18E+09	0.30%	9.98E+08	0.27%
26.22	1.14E+09	0.32%	9.55E+08	0.28%
26.54	1.09E+09	0.32%	9.11E+08	0.29%
26.85	1.05E+09	0.31%	8.69E+08	0.32%
27.17	1.00E+09	0.34%	8.28E+08	0.33%
27.49	9.63E+08	0.34%	7.90E+08	0.32%
27.81	9.23E+08	0.34%	7.54E+08	0.34%
28.13	8.84E+08	0.33%	7.21E+08	0.32%
28.44	8.46E+08	0.35%	6.88E+08	0.35%
28.76	8.10E+08	0.37%	6.55E+08	0.35%
29.08	7.76E+08	0.38%	6.24E+08	0.34%
29.40	7.45E+08	0.39%	5.97E+08	0.35%
29.71	7.16E+08	0.42%	5.70E+08	0.36%
30.03	6.84E+08	0.37%	5.44E+08	0.40%
30.35	6.54E+08	0.40%	5.19E+08	0.39%
30.67	6.29E+08	0.42%	4.95E+08	0.39%
30.99	6.02E+08	0.45%	4.74E+08	0.40%
31.30	5.77E+08	0.45%	4.53E+08	0.42%
31.62	5.53E+08	0.46%	4.35E+08	0.42%
31.94	5.30E+08	0.45%	4.16E+08	0.44%
32.26	5.09E+08	0.47%	3.97E+08	0.46%
32.57	4.86E+08	0.44%	3.79E+08	0.46%
32.89	4.66E+08	0.46%	3.62E+08	0.48%
33.21	4.47E+08	0.49%	3.47E+08	0.48%
33.53	4.28E+08	0.49%	3.33E+08	0.48%
33.85	4.09E+08	0.53%	3.19E+08	0.50%
34.16	3.91E+08	0.54%	3.04E+08	0.51%
34.48	3.76E+08	0.55%	2.90E+08	0.47%
34.80	3.60E+08	0.56%	2.79E+08	0.44%
35.12	3.47E+08	0.54%	2.66E+08	0.44%
35.43	3.33E+08	0.56%	2.54E+08	0.49%
35.75	3.21E+08	0.54%	2.42E+08	0.50%
36.07	3.10E+08	0.53%	2.33E+08	0.53%
36.39	2.97E+08	0.56%	2.23E+08	0.55%
36.71	2.85E+08	0.56%	2.13E+08	0.58%
37.02	2.72E+08	0.58%	2.04E+08	0.54%
37.34	2.61E+08	0.62%	1.94E+08	0.53%
37.66	2.49E+08	0.59%	1.86E+08	0.56%
37.98	2.42E+08	0.62%	1.78E+08	0.60%
38.29	2.31E+08	0.66%	1.71E+08	0.61%

38.61	2.21E+08	0.67%	1.66E+08	0.65%
38.93	2.12E+08	0.67%	1.58E+08	0.68%
39.25	2.05E+08	0.73%	1.51E+08	0.68%
39.57	1.97E+08	0.71%	1.45E+08	0.74%
39.88	1.88E+08	0.72%	1.38E+08	0.72%
40.20	1.82E+08	0.72%	1.33E+08	0.71%
40.52	1.76E+08	0.77%	1.27E+08	0.72%
40.84	1.68E+08	0.80%	1.21E+08	0.72%
41.15	1.60E+08	0.78%	1.17E+08	0.76%
41.47	1.54E+08	0.77%	1.11E+08	0.76%
41.79	1.47E+08	0.79%	1.07E+08	0.82%
42.11	1.43E+08	0.81%	1.03E+08	0.80%
42.43	1.38E+08	0.83%	9.79E+07	0.88%
42.74	1.33E+08	0.88%	9.37E+07	0.92%
43.06	1.28E+08	0.89%	8.97E+07	0.92%
43.38	1.23E+08	0.86%	8.64E+07	0.96%
43.70	1.19E+08	0.88%	8.27E+07	0.96%
44.01	1.14E+08	0.85%	8.01E+07	1.01%
44.33	1.10E+08	0.91%	7.66E+07	1.03%
44.65	1.05E+08	1.00%	7.40E+07	0.92%
44.97	1.01E+08	0.93%	7.14E+07	0.91%
45.29	9.70E+07	0.94%	6.80E+07	0.98%
45.60	9.28E+07	0.99%	6.51E+07	1.03%
45.92	8.82E+07	1.04%	6.22E+07	1.07%
46.24	8.50E+07	1.02%	6.01E+07	1.07%
46.56	8.18E+07	0.96%	5.86E+07	1.05%
46.88	7.86E+07	1.00%	5.54E+07	1.15%
47.19	7.50E+07	1.05%	5.35E+07	1.18%
47.51	7.17E+07	1.00%	5.16E+07	1.25%
47.83	7.00E+07	1.04%	4.97E+07	1.21%
48.15	6.73E+07	1.12%	4.75E+07	1.17%
48.46	6.46E+07	1.08%	4.54E+07	1.18%
48.78	6.20E+07	1.07%	4.37E+07	1.18%
49.10	6.01E+07	1.14%	4.15E+07	1.20%
49.42	5.77E+07	1.09%	4.01E+07	1.19%
49.74	5.62E+07	1.09%	3.86E+07	1.22%
50.05	5.36E+07	1.22%	3.73E+07	1.26%
50.37	5.18E+07	1.20%	3.63E+07	1.30%
50.69	5.02E+07	1.23%	3.49E+07	1.36%
51.01	4.82E+07	1.17%	3.31E+07	1.40%
51.32	4.63E+07	1.36%	3.19E+07	1.35%
51.64	4.43E+07	1.31%	3.05E+07	1.45%
51.96	4.29E+07	1.39%	2.90E+07	1.59%
52.28	4.11E+07	1.36%	2.80E+07	1.63%
52.60	3.95E+07	1.40%	2.68E+07	1.55%
52.91	3.75E+07	1.51%	2.57E+07	1.53%
53.23	3.68E+07	1.46%	2.47E+07	1.45%
53.55	3.51E+07	1.54%	2.41E+07	1.49%
53.87	3.35E+07	1.63%	2.29E+07	1.58%
54.18	3.19E+07	1.67%	2.20E+07	1.65%

54.50	3.07E+07	1.62%	2.12E+07	1.70%
54.82	2.96E+07	1.69%	2.05E+07	1.78%
55.14	2.87E+07	1.83%	1.96E+07	1.86%
55.46	2.72E+07	1.79%	1.89E+07	1.87%
55.77	2.64E+07	1.84%	1.80E+07	1.81%
56.09	2.56E+07	1.89%	1.74E+07	1.85%
56.41	2.39E+07	2.00%	1.71E+07	1.96%
56.73	2.33E+07	1.98%	1.64E+07	1.86%
57.04	2.27E+07	1.80%	1.56E+07	1.83%
57.36	2.20E+07	1.75%	1.47E+07	1.92%
57.68	2.11E+07	1.87%	1.41E+07	2.01%
58.00	2.02E+07	1.85%	1.39E+07	2.25%
58.32	1.90E+07	1.70%	1.30E+07	2.32%
58.63	1.84E+07	2.01%	1.25E+07	2.32%
58.95	1.79E+07	2.11%	1.21E+07	2.21%
59.27	1.71E+07	2.00%	1.18E+07	2.40%
59.59	1.66E+07	2.05%	1.14E+07	2.44%
59.90	1.62E+07	2.17%	1.10E+07	2.36%
60.22	1.54E+07	2.07%	1.07E+07	2.34%
60.54	1.49E+07	2.12%	1.01E+07	2.49%
60.86	1.45E+07	2.28%	9.50E+06	2.47%
61.18	1.43E+07	2.27%	9.30E+06	2.58%
61.49	1.40E+07	2.33%	9.10E+06	2.61%
61.81	1.36E+07	2.45%	8.60E+06	2.64%
62.13	1.28E+07	2.61%	8.40E+06	2.73%
62.45	1.24E+07	2.51%	8.10E+06	2.76%
62.76	1.18E+07	2.55%	7.80E+06	2.69%
63.08	1.12E+07	2.29%	7.30E+06	2.78%
63.40	1.09E+07	2.44%	7.00E+06	2.78%
63.72	1.01E+07	2.35%	6.60E+06	2.68%
64.04	1.00E+07	2.41%	6.40E+06	2.72%
64.35	9.50E+06	2.60%	6.00E+06	2.71%
64.67	9.00E+06	2.79%	5.90E+06	2.73%
64.99	8.80E+06	2.86%	6.00E+06	2.97%
65.31	8.50E+06	2.86%	5.50E+06	3.05%
65.63	8.30E+06	3.08%	5.50E+06	3.04%
65.94	7.90E+06	3.18%	5.10E+06	3.05%
66.26	7.50E+06	3.33%	4.90E+06	3.16%
66.58	7.50E+06	3.32%	4.90E+06	3.29%
66.90	7.10E+06	3.60%	4.70E+06	3.55%
67.21	6.70E+06	3.68%	4.50E+06	3.70%
67.53	6.40E+06	4.16%	4.20E+06	3.97%
67.85	6.20E+06	3.82%	4.10E+06	3.89%
68.17	6.00E+06	3.75%	3.90E+06	4.08%
68.49	5.60E+06	3.98%	3.60E+06	4.26%
68.80	5.30E+06	3.73%	3.30E+06	4.34%
69.12	5.30E+06	4.00%	3.20E+06	4.21%
69.44	4.90E+06	4.19%	3.10E+06	4.25%
69.76	4.60E+06	4.04%	2.80E+06	4.22%
70.07	4.30E+06	4.09%	2.60E+06	4.22%

70.39	4.00E+06	4.21%	2.50E+06	4.44%
70.71	3.90E+06	4.33%	2.30E+06	4.48%
71.03	3.60E+06	4.71%	2.20E+06	4.33%
71.35	3.40E+06	4.62%	2.10E+06	4.56%
71.66	3.20E+06	4.82%	1.80E+06	4.57%
71.98	2.80E+06	4.56%	1.70E+06	4.56%
72.30	2.50E+06	5.13%	1.60E+06	4.81%
72.62	2.30E+06	5.25%	1.50E+06	5.32%
72.93	2.10E+06	5.62%	1.30E+06	5.37%
73.25	1.70E+06	5.56%	1.20E+06	5.55%
73.57	1.60E+06	6.02%	1.10E+06	5.76%
73.89	1.30E+06	6.93%	9.00E+05	6.14%
74.21	1.10E+06	6.75%	8.00E+05	7.26%
74.52	8.00E+05	7.38%	6.00E+05	8.43%
74.84	5.00E+05	7.54%	4.00E+05	7.89%

Table C.3: Serpent2 output data for BF_3 detector

Fiber + Scintillator

	S1		S2	
Distance (cm)	RR_{sss2} $\frac{b \cdot cm}{s}$	ΔRR $\frac{b \cdot cm}{s}$	RR_{sss2} $\frac{b \cdot cm}{s}$	ΔRR $\frac{b \cdot cm}{s}$
0.06	7.000E+02	2.031E+02	1.000E+03	2.286E+02
0.17	2.200E+03	3.186E+02	2.600E+03	3.549E+02
0.28	3.500E+03	4.501E+02	4.400E+03	4.391E+02
0.40	5.300E+03	5.168E+02	6.300E+03	5.109E+02
0.51	7.000E+03	6.524E+02	7.400E+03	5.846E+02
0.62	1.040E+04	7.519E+02	1.050E+04	6.017E+02
0.73	9.500E+03	6.384E+02	1.300E+04	7.813E+02
0.85	1.370E+04	8.275E+02	1.520E+04	7.798E+02
0.96	1.600E+04	1.026E+03	1.910E+04	9.474E+02
1.07	1.720E+04	9.735E+02	2.020E+04	1.008E+03
1.19	2.330E+04	1.186E+03	2.500E+04	1.153E+03
1.30	2.780E+04	1.329E+03	3.450E+04	1.349E+03
1.41	5.230E+04	3.567E+03	5.370E+04	2.954E+03
1.52	6.400E+04	4.710E+03	7.360E+04	4.718E+03
1.64	8.210E+04	5.008E+03	9.360E+04	4.933E+03
1.75	1.107E+05	5.269E+03	1.237E+05	4.960E+03
1.86	1.392E+05	6.055E+03	1.624E+05	5.668E+03
1.98	1.804E+05	6.260E+03	1.932E+05	5.506E+03
2.09	2.276E+05	6.441E+03	2.761E+05	6.875E+03
2.20	2.956E+05	7.449E+03	3.178E+05	6.706E+03
2.31	3.377E+05	8.443E+03	3.898E+05	7.679E+03
2.43	4.065E+05	8.211E+03	4.475E+05	7.966E+03
2.54	4.469E+05	1.028E+04	5.074E+05	8.930E+03
2.65	4.889E+05	1.032E+04	5.762E+05	9.104E+03
2.77	5.447E+05	1.029E+04	5.950E+05	8.866E+03
2.88	6.002E+05	1.182E+04	6.754E+05	1.108E+04

2.99	6.228E+05	1.065E+04	7.115E+05	1.025E+04
3.10	6.862E+05	1.112E+04	7.825E+05	1.088E+04
3.22	7.503E+05	1.261E+04	8.346E+05	1.085E+04
3.33	7.858E+05	1.194E+04	8.776E+05	1.167E+04
3.44	8.174E+05	1.341E+04	9.140E+05	1.170E+04
3.56	8.749E+05	1.479E+04	9.670E+05	1.228E+04
3.67	9.269E+05	1.372E+04	1.020E+06	1.214E+04
3.78	9.290E+05	1.366E+04	1.051E+06	1.209E+04
3.89	9.635E+05	1.291E+04	1.105E+06	1.237E+04
4.01	1.046E+06	1.464E+04	1.104E+06	1.347E+04
4.12	1.047E+06	1.445E+04	1.182E+06	1.336E+04
4.23	1.101E+06	1.585E+04	1.191E+06	1.548E+04
4.35	1.121E+06	1.693E+04	1.261E+06	1.375E+04
4.46	1.138E+06	1.490E+04	1.268E+06	1.344E+04
4.57	1.195E+06	1.434E+04	1.325E+06	1.431E+04
4.68	1.219E+06	1.682E+04	1.378E+06	1.529E+04
4.80	1.262E+06	1.527E+04	1.374E+06	1.484E+04
4.91	1.257E+06	1.609E+04	1.445E+06	1.632E+04
5.02	1.295E+06	1.696E+04	1.455E+06	1.571E+04
5.14	1.291E+06	1.549E+04	1.475E+06	1.445E+04
5.25	1.354E+06	1.747E+04	1.495E+06	1.435E+04
5.36	1.352E+06	1.730E+04	1.517E+06	1.517E+04
5.47	1.388E+06	1.652E+04	1.542E+06	1.450E+04
5.59	1.367E+06	1.572E+04	1.547E+06	1.516E+04
5.70	1.388E+06	1.679E+04	1.579E+06	1.626E+04
5.81	1.412E+06	1.737E+04	1.592E+06	1.608E+04
5.93	1.465E+06	1.699E+04	1.606E+06	1.462E+04
6.04	1.467E+06	1.702E+04	1.615E+06	1.760E+04
6.15	1.446E+06	1.764E+04	1.594E+06	1.594E+04
6.26	1.475E+06	1.814E+04	1.643E+06	1.561E+04
6.38	1.478E+06	1.729E+04	1.626E+06	1.447E+04
6.49	1.503E+06	1.803E+04	1.646E+06	1.761E+04
6.60	1.481E+06	1.955E+04	1.658E+06	1.641E+04
6.72	1.518E+06	1.654E+04	1.644E+06	1.742E+04
6.83	1.490E+06	1.774E+04	1.653E+06	1.521E+04
6.94	1.525E+06	1.617E+04	1.664E+06	1.697E+04
7.05	1.515E+06	1.712E+04	1.680E+06	1.596E+04
7.17	1.537E+06	1.783E+04	1.683E+06	1.565E+04
7.28	1.526E+06	1.785E+04	1.675E+06	1.625E+04
7.39	1.525E+06	1.738E+04	1.651E+06	1.469E+04
7.51	1.529E+06	1.804E+04	1.679E+06	1.494E+04
7.62	1.522E+06	1.735E+04	1.699E+06	1.563E+04
7.73	1.519E+06	1.702E+04	1.645E+06	1.612E+04
7.84	1.527E+06	1.878E+04	1.653E+06	1.471E+04
7.96	1.527E+06	1.694E+04	1.682E+06	1.581E+04
8.07	1.508E+06	1.523E+04	1.662E+06	1.596E+04
8.18	1.516E+06	1.714E+04	1.651E+06	1.535E+04
8.30	1.500E+06	1.695E+04	1.656E+06	1.490E+04
8.41	1.518E+06	1.700E+04	1.669E+06	1.669E+04
8.52	1.491E+06	1.774E+04	1.624E+06	1.510E+04

8.63	1.497E+06	1.857E+04	1.620E+06	1.491E+04
8.75	1.453E+06	1.758E+04	1.620E+06	1.555E+04
8.86	1.473E+06	1.738E+04	1.574E+06	1.558E+04
8.97	1.471E+06	1.720E+04	1.565E+06	1.596E+04
9.09	1.439E+06	1.554E+04	1.595E+06	1.515E+04
9.20	1.444E+06	1.776E+04	1.551E+06	1.598E+04
9.31	1.421E+06	1.534E+04	1.557E+06	1.541E+04
9.42	1.418E+06	1.659E+04	1.582E+06	1.614E+04
9.54	1.385E+06	1.690E+04	1.555E+06	1.524E+04
9.65	1.386E+06	1.705E+04	1.513E+06	1.468E+04
9.76	1.405E+06	1.728E+04	1.514E+06	1.468E+04
9.88	1.374E+06	1.704E+04	1.482E+06	1.586E+04
9.99	1.359E+06	1.563E+04	1.477E+06	1.477E+04
10.10	1.329E+06	1.528E+04	1.477E+06	1.477E+04
10.21	1.338E+06	1.538E+04	1.421E+06	1.592E+04
10.33	1.327E+06	1.553E+04	1.406E+06	1.532E+04
10.44	1.324E+06	1.602E+04	1.418E+06	1.504E+04
10.55	1.292E+06	1.679E+04	1.377E+06	1.363E+04
10.67	1.283E+06	1.603E+04	1.378E+06	1.475E+04
10.78	1.266E+06	1.558E+04	1.345E+06	1.425E+04
10.89	1.293E+06	1.616E+04	1.332E+06	1.452E+04
11.00	1.253E+06	1.503E+04	1.316E+06	1.329E+04
11.12	1.213E+06	1.419E+04	1.299E+06	1.325E+04
11.23	1.225E+06	1.605E+04	1.264E+06	1.377E+04
11.34	1.202E+06	1.658E+04	1.279E+06	1.419E+04
11.46	1.227E+06	1.485E+04	1.244E+06	1.269E+04
11.57	1.169E+06	1.484E+04	1.248E+06	1.423E+04
11.68	1.147E+06	1.526E+04	1.240E+06	1.401E+04
11.79	1.160E+06	1.566E+04	1.195E+06	1.290E+04
11.91	1.132E+06	1.551E+04	1.197E+06	1.316E+04
12.02	1.136E+06	1.454E+04	1.195E+06	1.470E+04
12.13	1.115E+06	1.538E+04	1.141E+06	1.164E+04
12.25	1.083E+06	1.376E+04	1.151E+06	1.243E+04
12.36	1.055E+06	1.455E+04	1.109E+06	1.319E+04
12.47	1.071E+06	1.446E+04	1.118E+06	1.353E+04
12.58	1.038E+06	1.443E+04	1.097E+06	1.262E+04
12.70	1.033E+06	1.312E+04	1.079E+06	1.316E+04
12.81	1.039E+06	1.497E+04	1.037E+06	1.286E+04
12.92	9.980E+05	1.307E+04	1.039E+06	1.153E+04
13.04	9.944E+05	1.362E+04	1.036E+06	1.274E+04
13.15	9.591E+05	1.285E+04	9.963E+05	1.245E+04
13.26	9.615E+05	1.288E+04	9.830E+05	1.189E+04
13.37	9.432E+05	1.245E+04	9.726E+05	1.109E+04
13.49	9.235E+05	1.431E+04	9.705E+05	1.213E+04
13.60	9.165E+05	1.356E+04	9.397E+05	1.165E+04
13.71	9.034E+05	1.265E+04	9.246E+05	1.248E+04
13.83	8.862E+05	1.329E+04	9.138E+05	1.179E+04
13.94	8.870E+05	1.268E+04	9.028E+05	1.129E+04
14.05	8.877E+05	1.190E+04	8.885E+05	1.208E+04
14.16	8.506E+05	1.276E+04	8.608E+05	1.085E+04

14.28	8.551E+05	1.214E+04	8.611E+05	1.171E+04
14.39	8.384E+05	1.258E+04	8.584E+05	1.210E+04
14.50	8.230E+05	1.037E+04	8.339E+05	1.051E+04
14.62	8.217E+05	1.200E+04	8.376E+05	9.800E+03
14.73	7.854E+05	1.280E+04	8.021E+05	1.083E+04
14.84	7.792E+05	1.145E+04	7.772E+05	1.205E+04
14.95	7.569E+05	1.105E+04	7.632E+05	1.023E+04
15.07	7.655E+05	1.255E+04	7.745E+05	1.015E+04
15.18	7.503E+05	1.185E+04	7.608E+05	1.042E+04
15.29	7.364E+05	1.149E+04	7.405E+05	1.074E+04
15.41	7.228E+05	1.091E+04	7.248E+05	1.152E+04
15.52	7.224E+05	1.127E+04	7.192E+05	1.028E+04
15.63	6.844E+05	1.081E+04	7.081E+05	1.090E+04
15.74	7.048E+05	1.121E+04	6.879E+05	9.906E+03
15.86	6.749E+05	1.235E+04	6.964E+05	1.024E+04
15.97	6.586E+05	1.146E+04	6.742E+05	9.574E+03
16.08	6.623E+05	1.172E+04	6.631E+05	9.283E+03
16.20	6.590E+05	1.101E+04	6.394E+05	9.847E+03
16.31	6.620E+05	1.046E+04	6.487E+05	9.082E+03
16.42	6.346E+05	1.117E+04	6.272E+05	9.659E+03
16.54	6.125E+05	1.060E+04	6.152E+05	8.428E+03
16.65	5.988E+05	1.012E+04	6.001E+05	9.782E+03
16.76	6.089E+05	9.803E+03	5.852E+05	9.188E+03
16.87	6.020E+05	1.017E+04	5.824E+05	8.503E+03
16.99	6.081E+05	1.058E+04	5.711E+05	8.966E+03
17.10	5.867E+05	1.044E+04	5.812E+05	9.415E+03
17.21	5.886E+05	1.042E+04	5.326E+05	8.522E+03
17.33	5.562E+05	1.001E+04	5.370E+05	8.431E+03
17.44	5.468E+05	9.897E+03	5.194E+05	8.674E+03
17.55	5.432E+05	1.076E+04	5.209E+05	8.230E+03
17.66	5.324E+05	9.051E+03	5.145E+05	7.975E+03
17.78	5.348E+05	1.059E+04	5.015E+05	9.328E+03
17.89	5.035E+05	9.869E+03	5.048E+05	9.137E+03
18.00	4.862E+05	8.606E+03	4.875E+05	8.044E+03
18.12	4.909E+05	8.836E+03	4.795E+05	7.864E+03
18.23	4.998E+05	1.010E+04	4.822E+05	8.005E+03
18.34	4.869E+05	1.013E+04	4.539E+05	8.125E+03
18.45	4.820E+05	9.833E+03	4.395E+05	8.394E+03
18.57	4.655E+05	8.938E+03	4.293E+05	8.200E+03
18.68	4.619E+05	1.044E+04	4.259E+05	7.368E+03
18.79	4.420E+05	8.840E+03	4.154E+05	7.602E+03
18.91	4.230E+05	8.249E+03	4.230E+05	7.572E+03
19.02	4.207E+05	8.162E+03	4.088E+05	7.318E+03
19.13	4.307E+05	9.088E+03	4.036E+05	7.305E+03
19.24	4.073E+05	8.350E+03	3.941E+05	7.291E+03
19.36	4.086E+05	8.254E+03	3.870E+05	6.773E+03
19.47	3.942E+05	8.002E+03	3.935E+05	7.673E+03
19.58	4.226E+05	7.945E+03	3.642E+05	7.430E+03
19.70	3.836E+05	8.478E+03	3.767E+05	7.233E+03
19.81	3.732E+05	8.098E+03	3.611E+05	7.222E+03

19.92	3.819E+05	8.020E+03	3.677E+05	8.053E+03
20.03	3.850E+05	8.085E+03	3.421E+05	7.013E+03
20.15	3.596E+05	8.630E+03	3.409E+05	6.545E+03
20.26	3.504E+05	7.148E+03	3.316E+05	6.334E+03
20.37	3.743E+05	8.609E+03	3.250E+05	6.143E+03
20.49	3.421E+05	8.005E+03	3.264E+05	6.397E+03
20.60	3.425E+05	8.494E+03	3.185E+05	6.561E+03
20.71	3.354E+05	7.714E+03	3.182E+05	6.491E+03
20.82	3.315E+05	8.188E+03	3.138E+05	6.370E+03
20.94	3.291E+05	7.240E+03	3.024E+05	6.502E+03
21.05	3.119E+05	7.330E+03	2.912E+05	6.523E+03
21.16	3.227E+05	7.132E+03	2.906E+05	6.626E+03
21.28	3.129E+05	8.292E+03	2.848E+05	5.867E+03
21.39	3.129E+05	7.134E+03	2.906E+05	6.684E+03
21.50	2.899E+05	7.016E+03	2.731E+05	6.227E+03
21.61	2.967E+05	7.180E+03	2.747E+05	6.401E+03
21.73	2.991E+05	7.298E+03	2.658E+05	6.167E+03
21.84	2.891E+05	7.314E+03	2.622E+05	6.240E+03
21.95	2.816E+05	7.462E+03	2.424E+05	5.454E+03
22.07	2.757E+05	7.058E+03	2.530E+05	5.946E+03
22.18	2.836E+05	7.572E+03	2.386E+05	5.941E+03
22.29	2.696E+05	6.363E+03	2.401E+05	5.714E+03
22.40	2.671E+05	6.731E+03	2.363E+05	5.766E+03
22.52	2.661E+05	6.573E+03	2.248E+05	5.080E+03
22.63	2.480E+05	6.770E+03	2.314E+05	6.271E+03
22.74	2.600E+05	6.292E+03	2.233E+05	5.828E+03
22.86	2.442E+05	6.642E+03	2.243E+05	5.114E+03
22.97	2.491E+05	6.153E+03	2.076E+05	5.335E+03
23.08	2.414E+05	6.856E+03	2.167E+05	5.396E+03
23.19	2.442E+05	6.593E+03	2.093E+05	5.002E+03
23.31	2.303E+05	5.573E+03	2.004E+05	5.090E+03
23.42	2.272E+05	6.430E+03	1.978E+05	4.886E+03
23.53	2.103E+05	5.994E+03	1.987E+05	4.987E+03
23.65	2.342E+05	6.511E+03	1.871E+05	5.519E+03
23.76	2.222E+05	6.377E+03	1.825E+05	4.873E+03
23.87	2.169E+05	6.052E+03	1.817E+05	5.051E+03
23.98	2.072E+05	6.195E+03	1.819E+05	5.039E+03
24.10	2.204E+05	6.325E+03	1.725E+05	4.847E+03
24.21	2.164E+05	5.951E+03	1.727E+05	4.456E+03
24.32	2.032E+05	5.893E+03	1.664E+05	5.025E+03
24.44	2.025E+05	5.488E+03	1.738E+05	4.554E+03
24.55	1.888E+05	5.815E+03	1.630E+05	4.743E+03
24.66	2.006E+05	6.620E+03	1.607E+05	4.451E+03
24.77	1.968E+05	5.589E+03	1.614E+05	4.342E+03
24.89	1.874E+05	5.828E+03	1.572E+05	4.276E+03
25.00	1.768E+05	5.286E+03	1.501E+05	4.293E+03
25.11	1.856E+05	5.624E+03	1.490E+05	3.919E+03
25.23	1.715E+05	5.248E+03	1.442E+05	4.643E+03
25.34	1.760E+05	5.579E+03	1.510E+05	4.424E+03
25.45	1.730E+05	5.346E+03	1.430E+05	4.791E+03

25.56	1.656E+05	5.399E+03	1.442E+05	4.023E+03
25.68	1.647E+05	5.517E+03	1.387E+05	4.549E+03
25.79	1.668E+05	5.454E+03	1.409E+05	3.889E+03
25.90	1.630E+05	5.379E+03	1.318E+05	4.204E+03
26.02	1.525E+05	4.941E+03	1.322E+05	4.548E+03
26.13	1.556E+05	5.384E+03	1.341E+05	4.626E+03
26.24	1.522E+05	5.266E+03	1.198E+05	4.037E+03
26.35	1.567E+05	5.406E+03	1.307E+05	4.222E+03
26.47	1.487E+05	5.457E+03	1.243E+05	4.127E+03
26.58	1.399E+05	4.952E+03	1.218E+05	3.776E+03
26.69	1.367E+05	5.154E+03	1.125E+05	3.566E+03
26.81	1.363E+05	4.443E+03	1.230E+05	3.850E+03
26.92	1.454E+05	5.234E+03	1.194E+05	3.928E+03
27.03	1.427E+05	4.566E+03	1.111E+05	3.866E+03
27.14	1.362E+05	5.475E+03	1.042E+05	3.418E+03
27.26	1.324E+05	4.621E+03	1.046E+05	3.849E+03
27.37	1.311E+05	4.929E+03	1.087E+05	3.620E+03
27.48	1.214E+05	4.637E+03	1.056E+05	3.854E+03
27.60	1.329E+05	5.436E+03	1.036E+05	3.781E+03
27.71	1.269E+05	4.873E+03	1.052E+05	3.934E+03
27.82	1.232E+05	5.002E+03	1.044E+05	3.142E+03
27.93	1.143E+05	4.275E+03	1.070E+05	3.670E+03
28.05	1.189E+05	4.126E+03	9.570E+04	3.283E+03
28.16	1.170E+05	4.434E+03	1.013E+05	3.667E+03
28.27	1.099E+05	4.418E+03	9.390E+04	3.578E+03
28.39	1.108E+05	4.731E+03	9.350E+04	3.544E+03
28.50	1.122E+05	3.927E+03	9.150E+04	3.706E+03
28.61	9.860E+04	4.043E+03	9.050E+04	3.158E+03
28.72	1.063E+05	4.061E+03	8.830E+04	3.179E+03
28.84	1.066E+05	4.392E+03	8.850E+04	3.443E+03
28.95	1.061E+05	4.180E+03	8.930E+04	3.536E+03
29.06	1.095E+05	4.446E+03	8.350E+04	3.048E+03
29.18	1.070E+05	4.098E+03	8.370E+04	3.013E+03
29.29	1.091E+05	4.659E+03	7.700E+04	3.203E+03
29.40	9.870E+04	4.116E+03	7.390E+04	2.934E+03
29.51	1.027E+05	4.632E+03	7.910E+04	3.267E+03
29.63	9.450E+04	4.101E+03	7.570E+04	3.066E+03
29.74	1.020E+05	4.335E+03	7.620E+04	2.918E+03
29.85	9.510E+04	4.032E+03	7.190E+04	2.876E+03
29.97	9.000E+04	3.978E+03	7.540E+04	3.182E+03
30.08	9.470E+04	4.082E+03	7.470E+04	3.122E+03
30.19	9.420E+04	4.418E+03	7.220E+04	2.931E+03
30.30	8.960E+04	4.157E+03	7.130E+04	2.952E+03
30.42	8.700E+04	3.906E+03	6.880E+04	2.890E+03
30.53	8.850E+04	4.071E+03	7.140E+04	3.035E+03
30.64	8.820E+04	3.546E+03	6.190E+04	2.990E+03
30.76	8.030E+04	3.670E+03	6.510E+04	2.910E+03
30.87	8.430E+04	3.557E+03	5.870E+04	2.671E+03
30.98	7.480E+04	3.456E+03	6.120E+04	3.042E+03
31.09	7.970E+04	3.523E+03	6.470E+04	2.620E+03

31.21	7.930E+04	3.592E+03	6.110E+04	2.847E+03
31.32	7.430E+04	3.344E+03	6.140E+04	2.849E+03
31.43	7.520E+04	3.956E+03	6.070E+04	2.883E+03
31.55	7.730E+04	3.594E+03	6.000E+04	2.688E+03
31.66	7.610E+04	3.204E+03	5.430E+04	2.590E+03
31.77	6.760E+04	3.245E+03	5.400E+04	2.587E+03
31.88	7.000E+04	3.437E+03	5.680E+04	2.738E+03
32.00	6.780E+04	3.627E+03	5.320E+04	2.479E+03
32.11	7.170E+04	3.513E+03	5.320E+04	2.484E+03
32.22	6.370E+04	2.841E+03	5.360E+04	2.653E+03
32.34	6.950E+04	3.496E+03	5.170E+04	2.461E+03
32.45	7.110E+04	3.704E+03	4.980E+04	2.370E+03
32.56	6.160E+04	2.908E+03	4.720E+04	2.148E+03
32.67	6.960E+04	3.738E+03	5.000E+04	2.405E+03
32.79	5.890E+04	2.974E+03	5.090E+04	2.250E+03
32.90	6.050E+04	3.140E+03	4.690E+04	2.326E+03
33.01	5.670E+04	2.988E+03	5.080E+04	2.555E+03
33.13	5.540E+04	3.008E+03	4.970E+04	2.500E+03
33.24	5.890E+04	3.175E+03	4.430E+04	2.383E+03
33.35	5.640E+04	3.046E+03	4.620E+04	2.255E+03
33.47	5.510E+04	3.019E+03	4.370E+04	2.181E+03
33.58	5.760E+04	2.845E+03	4.150E+04	2.478E+03
33.69	5.820E+04	2.893E+03	4.120E+04	2.394E+03
33.80	5.150E+04	2.781E+03	3.930E+04	2.138E+03
33.92	5.310E+04	3.005E+03	4.320E+04	2.328E+03
34.03	5.390E+04	2.916E+03	3.980E+04	2.209E+03
34.14	5.590E+04	2.963E+03	4.180E+04	2.111E+03
34.26	4.660E+04	2.386E+03	4.020E+04	2.183E+03
34.37	5.350E+04	3.231E+03	3.510E+04	1.994E+03
34.48	4.740E+04	2.669E+03	3.720E+04	2.091E+03
34.59	5.250E+04	2.835E+03	3.720E+04	1.979E+03
34.71	5.010E+04	2.901E+03	3.780E+04	2.151E+03
34.82	4.940E+04	2.964E+03	3.820E+04	2.143E+03
34.93	4.350E+04	2.484E+03	3.560E+04	2.086E+03

Table C.4: Serpent2 output data Fiber+Scintillator

$^{3}\text{He}_{large}$

Distance (cm)	S1		S2	
	RR_{sss2} ($\frac{b \cdot cm}{s}$)	err (-)	RR_{sss2} ($\frac{b \cdot cm}{s}$)	err (-)
0.82	3.13E+09	0.42%	3.43E+09	0.31%
2.45	2.36E+10	0.13%	2.61E+10	0.11%
4.08	5.77E+10	0.11%	6.36E+10	0.08%
5.71	7.98E+10	0.09%	8.73E+10	0.07%
7.34	8.88E+10	0.08%	9.59E+10	0.08%
8.97	8.75E+10	0.09%	9.31E+10	0.08%
10.60	8.02E+10	0.09%	8.36E+10	0.08%
12.23	7.01E+10	0.10%	7.16E+10	0.08%
13.86	5.95E+10	0.10%	5.93E+10	0.09%
15.49	4.96E+10	0.12%	4.82E+10	0.10%
17.12	4.08E+10	0.12%	3.86E+10	0.11%
18.75	3.34E+10	0.13%	3.07E+10	0.13%
20.38	2.73E+10	0.13%	2.43E+10	0.14%
22.01	2.21E+10	0.17%	1.93E+10	0.16%
23.64	1.79E+10	0.18%	1.54E+10	0.18%
25.27	1.46E+10	0.21%	1.22E+10	0.18%
26.90	1.19E+10	0.21%	9.75E+09	0.21%
28.53	9.69E+09	0.22%	7.79E+09	0.25%
30.16	7.92E+09	0.26%	6.24E+09	0.27%
31.79	6.44E+09	0.28%	5.01E+09	0.27%
33.42	5.26E+09	0.32%	4.03E+09	0.33%
35.05	4.29E+09	0.36%	3.26E+09	0.35%
36.68	3.49E+09	0.39%	2.62E+09	0.40%
38.32	2.86E+09	0.40%	2.11E+09	0.43%
39.95	2.36E+09	0.46%	1.71E+09	0.48%
41.58	1.92E+09	0.51%	1.39E+09	0.55%
43.21	1.58E+09	0.53%	1.13E+09	0.57%
44.84	1.31E+09	0.57%	9.15E+08	0.63%
46.47	1.07E+09	0.63%	7.50E+08	0.69%
48.10	8.95E+08	0.71%	6.18E+08	0.75%
49.73	7.35E+08	0.78%	5.09E+08	0.85%
51.36	6.08E+08	0.93%	4.12E+08	0.91%
52.99	5.03E+08	0.94%	3.37E+08	1.03%
54.62	4.12E+08	0.99%	2.82E+08	1.15%
56.25	3.42E+08	1.15%	2.32E+08	1.21%
57.88	2.86E+08	1.26%	1.92E+08	1.32%
59.51	2.38E+08	1.39%	1.57E+08	1.54%
61.14	1.99E+08	1.46%	1.30E+08	1.67%
62.77	1.64E+08	1.62%	1.05E+08	1.75%
64.40	1.31E+08	1.84%	8.60E+07	1.88%
66.03	1.05E+08	2.01%	6.90E+07	2.02%
67.66	8.70E+07	2.19%	5.50E+07	2.29%
69.29	6.90E+07	2.59%	4.30E+07	2.79%
70.92	5.10E+07	2.73%	3.20E+07	2.89%
72.55	3.50E+07	3.02%	2.20E+07	3.19%
74.18	1.70E+07	3.57%	1.00E+07	3.92%

Table C.1: Serpent2 output data for $^{3}\text{He}_{large}$

^{3}He_*small*

Distance (cm)	S1 RR_{sss2} $fracb \cdot cms$	err (-)	S2 RR_{sss2} $fracb \cdot cms$	err (-)
0.80	2.66E+09	0.45%	2.93E+09	0.37%
2.39	2.06E+10	0.14%	2.30E+10	0.11%
3.99	5.18E+10	0.11%	5.75E+10	0.09%
5.59	7.25E+10	0.09%	8.00E+10	0.08%
7.18	8.10E+10	0.09%	8.85E+10	0.08%
8.78	8.01E+10	0.09%	8.63E+10	0.07%
10.37	7.35E+10	0.09%	7.78E+10	0.08%
11.97	6.43E+10	0.10%	6.67E+10	0.08%
13.56	5.44E+10	0.11%	5.53E+10	0.09%
15.16	4.51E+10	0.12%	4.47E+10	0.10%
16.76	3.70E+10	0.13%	3.57E+10	0.11%
18.35	3.01E+10	0.14%	2.83E+10	0.12%
19.95	2.43E+10	0.15%	2.22E+10	0.13%
21.54	1.96E+10	0.18%	1.75E+10	0.16%
23.14	1.58E+10	0.21%	1.38E+10	0.18%
24.73	1.27E+10	0.21%	1.08E+10	0.18%
26.33	1.03E+10	0.24%	8.55E+09	0.22%
27.93	8.30E+09	0.27%	6.77E+09	0.24%
29.52	6.72E+09	0.31%	5.36E+09	0.27%
31.12	5.44E+09	0.31%	4.28E+09	0.30%
32.71	4.39E+09	0.33%	3.41E+09	0.33%
34.31	3.55E+09	0.38%	2.73E+09	0.36%
35.90	2.88E+09	0.41%	2.19E+09	0.42%
37.50	2.34E+09	0.46%	1.77E+09	0.47%
39.10	1.91E+09	0.48%	1.43E+09	0.50%
40.69	1.56E+09	0.58%	1.15E+09	0.61%
42.29	1.28E+09	0.64%	9.27E+08	0.63%
43.88	1.05E+09	0.70%	7.46E+08	0.73%
45.48	8.56E+08	0.73%	6.06E+08	0.78%
47.07	7.10E+08	0.78%	4.92E+08	0.89%
48.67	5.87E+08	0.88%	4.06E+08	0.91%
50.27	4.87E+08	0.97%	3.31E+08	1.09%
51.86	3.96E+08	1.08%	2.73E+08	1.15%
53.46	3.35E+08	1.18%	2.24E+08	1.24%
55.05	2.72E+08	1.41%	1.80E+08	1.26%
56.65	2.27E+08	1.42%	1.46E+08	1.48%
58.24	1.87E+08	1.62%	1.20E+08	1.67%
59.84	1.53E+08	1.74%	9.80E+07	1.87%
61.44	1.25E+08	1.79%	7.90E+07	2.04%
63.03	1.03E+08	2.12%	6.40E+07	2.43%
64.63	8.40E+07	2.36%	5.40E+07	2.51%
66.22	6.80E+07	2.78%	4.30E+07	2.67%
67.82	5.60E+07	2.65%	3.70E+07	2.78%
69.41	4.50E+07	2.78%	2.80E+07	3.05%
71.01	3.30E+07	3.21%	2.20E+07	3.91%
72.61	2.30E+07	3.55%	1.50E+07	4.56%
74.20	9.00E+06	4.60%	6.00E+06	5.10%

Table C.2: Serpent2 output data ^{3}He$_{small}$

Bibliography

[1] G. von Dardel and N. G. Sjöstrand. "Diffusion Parameters of Thermal Neutrons in Water". In: *Phys. Rev.* 96 (5 Dec. 1954), pp. 1245–1249. DOI: `10.1103/PhysRev.96.1245`. URL: `https://link.aps.org/doi/10.1103/PhysRev.96.1245`.

[2] J. Dufek. *Monte Carlo Methods and Simulations in Nuclear Technology, SH2704, Introduction.* 2017.

[3] P. Frajtag et al. *Reactor Experiments Course - Theory and Measurements.* 1st ed. Internal report. 2016.

[4] Gordon R. Gilmore. "Statistics of Counting". In: *Practical Gamma-Ray Spectrometry.* John Wiley and Sons, Ltd, 2008. Chap. 5, pp. 101–129. ISBN: 9780470861981. DOI: `10.1002/9780470861981.ch5`. eprint: `https://onlinelibrary.wiley.com/doi/pdf/10.1002/9780470861981.ch5`. URL: `https://onlinelibrary.wiley.com/doi/abs/10.1002/9780470861981.ch5`.

[5] J. Leppänen et al. *Serpent – a Continuous-energy Monte Carlo Reactor Physics Burnup Calculation Code.* Serpent's user manual. VTT Technical Research Centre of Finland. June 2015.

[6] J. Leppänen et al. *The Serpent Monte Carlo code: Status, development and applications in 2013.* 2015. URL: `http://montecarlo.vtt.fi/`.

[7] William H.Bond M.Edward Anderson. "Neutron spectrum of a plutonium-beryllium source". In: *Nuclear Physics* 43 (1963). ISSN 0029-5582, pp. 330–338.

[8] MATLAB. *version 9.5.0 (R2018b).* Natick, Massachusetts: The MathWorks Inc., 2018.

[9] ORTEC. *MAESTRO-32 MCA Emulator for Microsoft Windows 2000 Professional and XP Professional.* 6th ed. Software User's Manual. ORTEC. Sept. 2008.

[10] O.V. Pakari. "Development of Current and Fast Neutron Noise Measurements in CROCUS". MA thesis. EPFL, Aug. 2016.

[11] L. Stewart. "Neutron Spectrum and Absolute Yield of a Plutonium-Beryllium Source". In: *American Phisical Society* (1955). PhysRev.98.740 , DOI:10.1103/PhysRev.98.740.

[12] F. Vitullo et al. "Developing and testing a miniature fiber-coupled scintillator for in-core neutron counting in CROCUS". In: (2019).